7   **Benthic macrofaunal carbon fluxes and environmental drivers of spatial variability in a**

8   **large coastal-plain estuary**

9   Authors: Seyi Ajayi[1*], Raymond Najjar[1], Emily Rivest[2], Ryan Woodland[3], Marjorie A.M.

10   Friedrichs[2], Pierre St-Laurent[2], Spencer Davis[1]

11   [1]The Pennsylvania State University, University Park, PA, USA

12   [2]Virginia Institute of Marine Science, William & Mary, Gloucester Point, VA, USA

13   [3]University of Maryland Center for Environmental Sciences, Cambridge, MD, USA

14   *Correspondence to*: Seyi Ajayi (oaa5061@psu.edu)

Abstract

While the importance of carbon cycling in estuaries is increasingly recognized, the role of benthic macrofauna remains poorly quantified due to limited spatial and temporal resolution in biomass measurements. Here, we ask: (1) To what extent do benthic macrofauna contribute to estuarine carbon cycling via respiration and calcification? and (2) How well can routinely collected environmental variables predict their biomass? We analyzed data from 8,128 benthic samples collected from the Chesapeake Bay between 1995 and 2022 and estimated associated carbon fluxes using empirical relationships. We then used generalized additive models to relate observed and modeled environmental variables to the biomass. Biomass was highest in the upper main stem of the Bay (Upper Bay) and upper Potomac River Estuary, the largest tidal tributary of the Bay. In the Upper Bay, benthic macrofauna respired 18–45% of the estimated organic carbon supply. Calcification-driven alkalinity reduction reached 6.31 ± 2.84 mol m^{-2} yr^{-1} in the Potomac River Estuary, aligning with prior estimates of alkalinity sinks in the tributary and highlighting the potential importance of calcifying fauna in alkalinity dynamics. Estimated CO_2 production in the Upper Bay from benthic respiration and calcification (151 g C m^{-2} yr^{-1}) also exceeded observed air–sea CO_2 fluxes (74.5 g C m^{-2} yr^{-1}). Generalized additive models revealed that low salinity, moderate dissolved oxygen, and elevated nitrate best predicted high-biomass zones, with the three predictors explaining 52% of biomass deviance. These predictive relationships offer a pathway to estimate macrofaunal biomass and associated carbon fluxes in systems where direct biomass measurements are sparse. Our findings demonstrate that benthic macrofauna play a substantial and spatially structured role in estuarine carbon cycling. Incorporating their contributions into estuarine biogeochemical models will improve predictions of ecosystem responses to environmental and anthropogenic change.

1. Introduction

Benthic macrofauna are vitally important to estuarine ecosystems by improving water quality, producing and consuming organic matter, recycling nutrients, cycling pollutants, stabilizing and transporting sediment, and providing food for both human populations and estuarine organisms (Schratzberger & Ingels, 2018; Snelgrove, 1997; Wilson & Fleeger, 2023). Benthic macrofauna also play a role in estuarine carbon cycling through second production, respiration, and calcification. Secondary production refers to the consumption of organic matter by benthos to produce soft tissue biomass (Diaz & Schaffner, 1990; Dolbeth et al., 2012; Sturdivant et al., 2013). This biomass contributes to trophic transfer, as benthic organisms are consumed by predators or decomposers, with much of the associated organic carbon eventually being removed from the estuary through advection to the open ocean or burial in sediment (Diaz & Schaffner, 1990; Wilson & Fleeger, 2023). Respiration and calcification influence carbon cycling through their impact on the carbonate system, the chemical equilibrium governing the partitioning of inorganic carbon among its primary forms.

Impacts of respiration and calcification on the carbonate system are best understood via their impacts on two master variables, dissolved inorganic carbon (DIC) and total alkalinity (TA). DIC is a measure of the total concentration of inorganic carbon species in water, including CO_2, bicarbonate ion, and carbonate ion:

$$[DIC] = [CO_2] + [HCO_3^-] + [CO_3^{2-}]. \tag{1}$$

TA is the excess of proton acceptors over donors and reflects the capacity of a water body to buffer pH changes. For understanding impacts of biogeochemical processes, the form of TA known as the explicit conservative alkalinity (Glud, 2008; Wolf-Gladrow et al., 2007) is useful:

$$[TA] = [Na^+] + 2[Mg^{2+}] + 2[Ca^{2+}] + [K^+] + 2[Sr^{2+}] + \ldots - [Cl^-] - [Br^-] - [NO_3^-] - \ldots \\ - TPO_4 + TNH_3 - 2TSO_4 - THF - THNO_2, \tag{2}$$

71   where the last five terms represent the total forms of phosphate, ammonia, sulfate, fluoride, and

72   nitrite, respectively.

73   Respiration, unlike secondary production, directly alters the carbonate system.

74   Respiration is the metabolic process by which organisms break down organic matter to release

75   energy. Aerobic respiration, produces carbon dioxide (CO_2), water, and energy with oxygen

76   serving as the terminal electron acceptor:

77    $$CH_2O + O_2 \rightarrow CO_2 + H_2O. \tag{3}$$

78   When oxygen becomes depleted, anaerobic respiration takes over, relying on alternative electron

79   acceptors such as nitrate, sulfate, or iron oxides. For benthic macrofauna, oxygen is essential for

80   respiration; anaerobic respiration in sediments is primarily mediated by microbes (Glud, 2008).

81   The CO_2 generated during aerobic respiration increases DIC (Equation 1). Although aerobic

82   respiration slightly decreases TA due to the regeneration of nitrate during organic matter

83   remineralization, the effect is small ($\approx$16 moles of NO_3^- per 106 moles of CO_2; Redfield, 1963).

84   During calcification, benthic organisms, such as bivalves, take up calcium (Ca^{2+}) and

85   HCO_3^- to form calcium carbonate ($CaCO_3$) shells, releasing CO_2 and water as byproducts:

86    $$Ca^{2+} + 2HCO_3^- \rightarrow CaCO_3 + CO_2 + H_2O. \tag{4}$$

87   Although calcification increases CO_2 in the water column, it results in a net decrease in DIC,

88   since two moles of HCO_3^- are removed for every mole of $CaCO_3$ precipitated, while only one

89   mole of CO_2 is returned to the water column (Equation 1). The removal of Ca^{2+} also decreases

90   TA by twice the amount of DIC (Equation 2). Calcification is thermodynamically favored when

91   the calcium carbonate saturation state (Ω) exceeds 1. When $\Omega < 1$ (undersaturation), dissolution

92   is favored, leading to the release of Ca^{2+} and CO_3^{2-} back into solution and increasing TA. Low Ω

93   impairs shell formation and increases mortality in juveniles, regardless of pH or $p\mathrm{CO_2}$ (Green et

94   al., 2009; Thomsen et al., 2015; Waldbusser et al., 2015).

95   Building on these conceptual and mechanistic insights, field and modeling studies have

96   revealed the potentially large influence of benthic macrofauna on estuarine carbon cycling,

97   particularly through respiration and calcification. A compilation of data from 20 estuaries

98   estimated that benthos (encompassing microbes, meiofauna, and macrofauna) respire

99   approximately 24% of the total input of organic carbon, defined here as the sum of inputs of

100   autochthonous (from primary production) and allochthonous (e.g., from rivers) organic carbon,

101   (Hopkinson & Smith, 2004). An excess of benthic respiration over primary production observed

102   in many estuaries implies significant allochthonous inputs (Hopkinson & Smith, 2004; Kemp et

103   al., 1997; Schwinghamer et al., 1986). Benthic macrofauna, particularly bivalves, substantially

104   contribute to benthic respiration and have been hypothesized to significantly decrease the

105   phytoplankton and suspended particulate concentrations in estuaries (Cerco & Noel, 2010;

106   Galimany et al., 2020; Nakamura & Kerciku, 2000; Newell & Ott, 2011).

107   In contrast to respiration, the impact of benthic calcification on estuarine carbon cycling

108   remains underexplored (Waldbusser et al., 2013). However, large alkalinity sinks in estuarine

109   tributaries suggest that calcifying organisms, such as bivalves, may play a substantial role (Najjar

110   et al., 2020). The combined $\mathrm{CO_2}$ production from respiration and calcification may also

111   constitute a significant carbon flux to the atmosphere. In San Francisco Bay, this production is

112   estimated to occur at twice the rate of $\mathrm{CO_2}$ uptake by primary production, while global

113   extrapolations indicate that these emissions may rival those from the world's lakes or planetary

114   volcanism (Chauvaud et al., 2003). As previously described, although both respiration and

115   calcification generate $\mathrm{CO_2}$, they have opposite effects on DIC: respiration increases DIC,

116 whereas calcification reduces it. Thus whether calcifying benthos act as a net source or sink of

117 DIC depends on the relative magnitudes of these two processes.

118   To quantify the magnitude of these benthic contributions to carbon cycling, researchers

119 often estimate rates of secondary production, respiration, and calcification based on benthic

120 biomass. Because secondary production can be time-consuming and costly to measure, it is often

121 estimated using empirical relationships that relate it to benthic biomass, incorporating variables

122 such as taxon, average body mass, and water temperature (Brey, 1990; Chauvaud et al., 2003;

123 Dolbeth et al., 2012; Edgar, 1990; Schwinghamer et al., 1986; Sturdivant et al., 2013; Tumbiolo

124 & Downing, 1994). Calcification and respiration rates can be inferred from these secondary

125 production estimates using empirical relationships or proportional scaling (Chauvaud et al.,

126 2003; Schwinghamer et al., 1986).

127   Despite their importance to carbon cycling, benthic macrofauna biomass is rarely

128 measured due to high cost and logistical challenges (Pearson & Rosenberg, 1978; Snelgrove et

129 al., 2018). In contrast, environmental variables that influence benthic communities are typically

130 measured more frequently. To better incorporate benthic macrofaunal processes into carbon

131 budgets and numerical models, it is useful to assess how well these more readily available

132 environmental variables can serve as predictors of biomass.

133   There are many environmental influences on the distribution of benthic macrofauna.

134 Hypoxia (dissolved oxygen concentrations ≤ 2 mg L^{-1}) is a major stressor that reduces biomass,

135 alters community structure, and impairs key functions such as metabolism, bioturbation, and

136 calcification (Borja et al., 2008; Diaz et al., 1995; Diaz & Rosenberg, 2008; Levin et al., 2009;

137 Murphy et al., 2011; Rousi et al., 2019; Seitz et al., 2009; Woodland & Testa, 2020). Benthic

138 macrofauna are particularly vulnerable due to their proximity to the sediment–water interface,

139   immobility, and limited capacity to avoid low-oxygen zones (Dauer & Alden, 1995; Vaquer-

140   Sunyer & Duarte, 2008). Behavioral and physiological responses to hypoxia differ among taxa,

141   with some groups like bivalves showing greater tolerance to short-term events (Seitz et al., 2009;

142   Vaquer-Sunyer & Duarte, 2008; Woodland & Testa, 2020). Salinity also plays a central role in

143   structuring benthic communities, with species distributions reflecting distinct physiological

144   tolerances (Dauer, 1993; Holland et al., 1987; Little et al., 2017; Seitz et al., 2009; Sturdivant et

145   al., 2013). Ocean acidification has been shown to negatively impact calcifying taxa, particularly

146   mollusks, by reducing growth, survival, and development (Birchenough et al., 2015; Jakubowska

147   & Normant-Saremba, 2015; Jansson et al., 2013; Kroeker et al., 2013; Thomsen et al., 2015).

148   Sediment characteristics also influence benthic biomass and diversity. Finer grain sizes and

149   higher organic content tend to be associated with lower biomass and biodiversity, whereas sandy

150   sediments are generally more favorable (Dauer & Alden, 1995; Grebmeier et al., 2015; Seitz et

151   al., 2009; Woodland & Testa, 2020). Finally, food availability, primarily from phytoplankton

152   production, strongly governs benthic biomass (Ehrnsten et al., 2019; Hagy, 2002; Kemp et al.,

153   2005; Pearson & Rosenberg, 1978). However, the relationship is complex, as high primary

154   production can also lead to oxygen depletion that ultimately suppresses benthic communities

155   (Dauer et al., 2000; Kemp et al., 2005). In summary, dissolved oxygen, salinity, carbonate

156   chemistry, sediment composition, and food availability all serve as important environmental

157   predictors of benthic macrofauna biomass in estuarine ecosystems.

158   While numerous studies have examined the environmental drivers of benthic biomass in

159   estuaries, most have focused on relatively small spatial or temporal scales. Biomass, as opposed

160   to other metrics such as diversity and abundance, is particularly important because it is most

161   directly related to estuarine carbon cycling processes (Cerco & Noel, 2010; Snelgrove, 1999).

162 While benthic respiration has been widely quantified, estimates of benthic calcification remain

163 rare (e.g., Chauvaud et al., 2003; Waldbusser et al., 2013), limiting our understanding of benthic

164 contributions to carbon and alkalinity dynamics. The Chesapeake Bay, a large, coastal-plain

165 estuary in the eastern United States (Fig. 1), provides a valuable case study due to its extensive

166 historical monitoring data and diversity of carbon and alkalinity dynamics across its several tidal

167 tributaries (Najjar et al., 2020). Although prior studies in the Bay have linked environmental

168 variables to benthic biomass (Seitz et al., 2009; Woodland et al., 2021), these studies either used

169 older datasets or focused on biomass primarily as a food source for higher trophic levels.

170
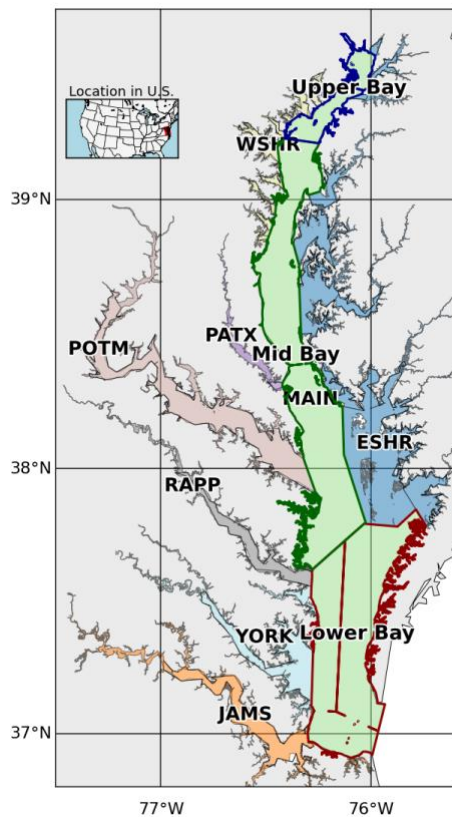
171 Figure 1: Segmentation of the mainstem of the Chesapeake Bay and its tidal tributaries. The

172 mainstem is divided into three regions, Upper Bay, Mid Bay, and Lower Bay. Acronyms denote

173 specific tributaries and sub-estuarine areas: ESHR refers to Eastern Shore tributaries, WSHR to

174 Western Shore tributaries, POTM to the Potomac River, PATX to the Patuxent River, RAPP to

175   the Rappahannock River, YORK to the York River system (including the Mattaponi and

176   Pamunkey Rivers), and JAMS to the James River.

177   In our study, we build on this previous work by addressing the following research

178   questions in the context of the Chesapeake Bay:

179   1) To what extent do benthic macrofauna contribute to estuarine carbon cycling through

180   respiration and calcification, and how might these contributions vary across space?

181   2) How well can environmental variables routinely collected in estuarine monitoring

182   programs predict benthic macrofauna biomass?

183   Answering these questions will help clarify the role of benthic macrofauna in estuarine carbon

184   cycling and improve the ability of monitoring programs and numerical models to account for

185   benthic processes using more accessible environmental data.

186   **2. Methods**

187   *2.1 Overview*

188   We examined historic benthic macrofauna biomass data collected annually by the

189   Chesapeake Bay Long-Term Benthic Monitoring Program (BMP) (Dauer et al., 2000; Llansó &

190   Zaveta, 2017). We applied empirical relationships linking biomass to secondary production,

191   respiration, and calcification to quantify the impact of benthic macrofauna on carbon cycling in

192   the Bay. To identify environmental predictors of benthic biomass, we compiled measurements of

193   bottom water temperature, salinity, dissolved oxygen, and sediment sand fraction measured by

194   the BMP at the same time and location as the benthic biomass samples. In addition to these

195   measured environmental variables, we utilized output from ROMS-ECB, which is a three-

196   dimensional estuarine carbon and biogeochemistry (ECB) model embedded into the Regional

197   Ocean Modeling System (ROMS; Shchepetkin & McWilliams, 2005) developed for the

198   Chesapeake Bay (St-Laurent & Friedrichs, 2024b). We identified correlations between these

199   environmental variables (observed and modeled) and benthic macrofauna biomass using

200   generalized additive models (GAMs).

201   ***2.2 Benthic biomass data***

202   Details of the BMP data we used in our study are described elsewhere (Dauer, 1993;

203   Dauer et al., 2000; Dauer & Lane, 2010; Llansó & Scott, 2011; Llansó & Zaveta, 2017) and are

204   summarized here. The program began in 1984, but consistency in sampling started in 1995. The

205   sampling occurs mainly in the summer, between July 15 and September 30, at both fixed and

206   random stations, with the latter changing location every year. The sampling is conducted

207   separately by the states of Maryland (Llansó & Zaveta, 2017) and Virginia (Dauer & Lane,

208   2010), with slightly different protocols used in each state (see below). Our analysis spanned 1995

209   to 2022, the recent extent of available data, incorporating 28 years of data.

210   The Maryland monitoring program comprises 27 fixed and 150 random stations in the

211   upper Chesapeake Bay. The Virginia monitoring program comprises 21 fixed and 100 random

212   stations in the lower Chesapeake Bay. In Virginia, random stations were not sampled in 1995,

213   and fixed stations were not sampled in 2017 or 2018. Water depths greater than 12 m in the

214   mainstem part of the Bay in Maryland are not sampled because the bottom waters become anoxic

215   in the summer, resulting in azoic sediments. The tributaries are sampled only in the tidal zone;

216   areas with less than 1 m mean lower low water are considered non-tidal. Some locations, such as

217   oyster reefs and other hard substrates, are also not sampled due to gear unsuitability in such

218   habitats. To avoid seasonal biases, we excluded samples collected outside of the summer

219   sampling window of July 15–September 30, which occurred earlier in the study period. This

220   selection resulted in a dataset of 8128 samples across both states, or an average of 290 samples

221   per year, slightly less than the maximum of 298.

222   At each sampling station, the uppermost layers of sediment are collected. In Maryland,

223   the sites introduced in 1995 (two fixed sites and all random sites) are sampled with a Young

224   grab, which collects a surface area of 0.0440 m^2 to a depth of 0.10 m. For the other fixed sites in

225   Maryland, nearshore shallow sandy habitats of the mainstem and tributaries are sampled with a

226   modified box corer with a surface area of 0.0250 m^2 to a depth of 0.25 m. Muddy habitats and

227   deep-water habitats in the mainstem and tributaries of Maryland are sampled with a Wildco box

228   corer with a surface area of 0.0225 m^2 to a depth of 0.23 m. The fixed site in the Nanticoke River

229   is sampled with a Petite Ponar grab with a surface area of 0.0250 m^2 to a depth of 0.07 m. In

230   Virginia, fixed sites use a spade-type box-coring device with a surface area of 0.0182 m^2 to a

231   depth of 0.02 m; random sites use a Young grab with a surface area of 0.0400 m^2 to a depth of

232   0.10 m. One limitation of using multiple types of sampling gear is that differences in design,

233   such as penetration depth, sample volume, and sediment disturbance, can introduce variability in

234   estimates of benthic diversity, abundance, and biomass (Eleftheriou & Moore, 2013).

235   For both monitoring programs, the sampling contents are sieved through a 0.5 mm screen

236   to retain only benthic macrofauna. The macrofauna are identified at the lowest taxonomical

237   level. The specimens are dried on a pan for at least 24 hours to a constant weight, then a final

238   weight is measured. The specimens are then placed in a muffle furnace for 4 hours at 500 °C for

239   ashing, and the specimens are weighed again. The ash-free dry weight (AFDW), representing

240   only the soft-tissue biomass, is the difference between the dry and ashed weight. We converted

241   the AFDW in g per sample to biomass density B in units of g m^{-2} by dividing the AFDW by the

242   area of the sampling device. The data used in our subsequent statistical analysis include the

243   biomass density of individually selected species and classes and the total biomass density.

244   Benthic biomass is known to be highly patchy, with large variability even between

245   samples taken in close proximity, hence the common use of replicate sampling in field protocols.

246   To mitigate this noise and extract meaningful large-scale spatial patterns, we averaged across the

247   28-year time frame. All 8128 biomass samples collected from 1995 to 2022 were averaged onto

248   a uniform grid with cells each measuring 0.04° in longitude and 0.03125° in latitude (~3.5 km

249   per side). 1295 cells had at least one biomass measurement during the 28-year period. Across

250   these cells, the average number of samples was 6.19, the median was 3, and the maximum was

251   69. Tributaries and the upper Bay were sampled more densely than the mainstem (Appendix A

252   and Fig. A1). This "time-averaging" approach enabled clearer interpretation of spatial gradients

253   in biomass and strengthened the robustness of subsequent statistical analyses aimed at

254   identifying consistent environmental drivers. Some benthic biomass sampling stations fell

255   outside the Chesapeake Bay Program (CBP) water quality segmentation scheme, which was

256   originally developed to support monitoring and management analyses (Chesapeake Bay Program

257   Analytical Segmentation Scheme: Revisions, Decisions and Rationales, 1983–2003, 2004). The

258   CBP segments are defined at a relatively coarse spatial scale and often exclude narrow nearshore

259   environments and small tributary creeks. To maintain consistency with the spatial framework

260   used in coupled hydrodynamic–biogeochemical models, in our case ROMS-ECB, we excluded

261   these points from analysis. This filtering step ensured that all biomass observations were aligned

262   with the modeled domain, avoiding mismatches at the land–water interface. After this step, 1008

263   grid cells remained, of which 868 contained at least one biomass observation and the remainder

264   were empty cells.

265 **_2.3 Carbon flux estimations_**

266   To estimate the impact of benthic macrofauna on carbon cycling, we applied empirical

267 equations from the literature to quantify secondary production, calcification, and respiration.

268 These equations were identified through an informal literature review using online tools (e.g.,

269 Google Scholar), with emphasis on studies relevant to soft-sediment bivalves, the dominant

270 macrofauna in the Chesapeake Bay. We prioritized relationships applicable to local taxa and

271 easily scalable to our biomass dataset. While multiple sources were available for secondary

272 production, equations for respiration and calcification were more limited; in those cases, we

273 selected models based on representative species that could be scaled from production estimates.

274 We used a range of published values for biomass-to-carbon conversion, secondary production,

275 and species-specific respiration and calcification ratios to estimate upper and lower bounds of

276 carbon fluxes. Additional details on uncertainty calculations are provided in the Appendix B.

277 *2.3.1 Secondary production*

278   We converted biomass to secondary production S (units of g C m^{-2} yr^{-1}). Multiple

279 approaches have been used for this conversion, and we used the average of three approaches to

280 be able to broadly quantify uncertainty in our estimates.

281   In the first approach, secondary production is given by:

282 $S_1 = \alpha B_c$ (5)

283 where α is the specific growth rate and B_c is carbon-based biomass (units of g C m^{-2}). We found

284 three studies that estimated α for benthic macrofauna. At the low end, a study of benthic

285 macrofauna in the Chesapeake Bay used $\alpha = 1.06$ yr^{-1} (Wilson & Fleeger, 2023). At the high

286 end, a study of *C. fluminea* used $\alpha = 4.45$ yr^{-1} (Chauvaud et al., 2003). An intermediate value of

287 $\alpha = 2$ yr^{-1} was based on monthly observations of benthic macrofauna dominated by the

288   crustacean *Corophium volutator* and the bivalve *Limecola balthica* at an intertidal site in the

289   upper Bay of Fundy (Schwinghamer et al., 1986). A mean value of 2.50 yr^{-1} was used in

290   Equation 5. B_c is computed from biomass B (units of g m^{-2}) using:

291      $B_c = r_c B$ (6)

292   where r_c is the ratio of carbon mass to total mass in benthic organic matter. In a study on the

293   bivalve filter feeders *Rangia cuneata* and *Corbicula fluminea*, which dominate in the tidal fresh

294   and oligohaline waters of the Chesapeake Bay, $r_c = 0.47$ g C g^{-1} was used (Cerco & Noel,

295   2010). A slightly lower value of 0.41 g C g^{-1} was used in a study of native and introduced

296   bivalves in six North American freshwater systems (Chauvaud et al., 2003). A mean value of r_c

297      $= 0.44$ g C g^{-1} was used in our calculation.

298   In the second approach, temperature (T) dependence for bivalve secondary production

299   was added (Sturdivant et al., 2013):

300      $S_2 = S_0 \left(\dfrac{B}{1 \text{ g m}^{-2}} \right)^{0.87} \left(\dfrac{T}{1 \text{ °C}} \right)^{0.46}$ (7)

301   where $S_0 = 0.40$ g C m^{-2} yr^{-1}. Note that the coefficient at the beginning of the equation differs

302   from that of Sturdivant et al. (2013) because of a change in units of B from mg to g m^{-2} and of S

303   from mg C d^{-1} to g C m^{-2} yr^{-1}. This equation has been shown to agree well with secondary

304   production and biomass measurements (Sturdivant et al., 2013).

305   Finally, in the third approach (Tumbiolo & Downing, 1994), depth (Z) dependence was

306   added:

307 $\log_{10}\left(\dfrac{S_3}{1\ \text{g C m}^{-2}\ \text{yr}^{-1}}\right)$

308 $= \beta_0 + b\ \log_{10}\left(\dfrac{B}{1\ \text{g m}^{-2}}\right) - m\ \log_{10}\left(\dfrac{M}{1\ \text{mg}}\right) + t\left(\dfrac{T}{1\ ^\circ\text{C}}\right)$

309 $-\ z\ \log_{10}\left(\dfrac{Z}{1\ \text{m}} + 1\right)$ (8)

310 where $\beta_0 = 0.24, b = 0.96, m = 0.21, t = 0.03, z = 0.16$, and M is the maximum individual

311 body mass. Equation 8 was developed by Tumbiolo & Downing (1994) through multiple

312 regression analysis of 125 benthic invertebrate populations, including data from the Chesapeake

313 Bay. In their model, M refers to the maximum individual mass of the largest size class observed

314 within a population. It was identified as the second most important predictor of secondary

315 production after total biomass. Their analysis showed that species with greater maximum sizes

316 tend to have slower turnover rates and lower production-to-biomass ratios. In our application, we

317 treated M as a constant, based on the maximum individual mass of the bivalve *R. cuneata*

318 collected in a study in the Choptank River in the Chesapeake Bay, which was 5953 mg (Hartwell

319 et al., 1991). *R. cuneata* is among the most abundant and largest benthic macrofaunal species in

320 our study area (Cerco & Noel, 2010; Hartwell et al., 1991).

321   In Equations 7 and 8, we used the bottom water temperature measured on the same day

322 the benthic samples were collected. This reliance on summer temperature values represents a key

323 limitation of our study, as it likely leads to overestimation of annual secondary production,

324 particularly for Equation 8. For example, Equations 7 and 8 both predict maximum summer

325 secondary production that is about 5 times larger than the minimum winter production, assuming

326 an annual temperature range of 1 °C to 25 °C. However, we note that the first approach for

327 secondary production (Equation 6) has no temperature dependence. Figures C1–C3 in Appendix

328   C provide a detailed comparison of secondary production across the three models and assess

329   temperature effects on Models 2 and 3.

330   *2.3.2 Calcification*

331   Benthic macrofaunal calcification C (g CaCO$_3$ m^{-2} yr^{-1}) was computed from secondary

332   production following Chauvaud et al. (2003):

333    $C = r_s S$ (9)

334   where r_s is the ratio of shell CaCO$_3$ mass production to tissue organic C mass production, which

335   has units of g CaCO$_3$ (g C)$^{-1}$. Based on samples of the bivalve *Potamocorbula amurensis* in the

336   northern San Francisco Bay, Chauvaud et al. (2003) found r_s to be 10 g CaCO$_3$ (g C)$^{-1}$. They

337   also cited a ratio of 15 g CaCO$_3$ (g C)$^{-1}$ for the bivalve *C. fluminea*, a more relevant species to

338   our study, but the reference is from unpublished data. We used the average of the two values,

339   12.5 g CaCO$_3$ (g C)$^{-1}$, which corresponds to a molar ratio of 1.5 mol CaCO$_3$ (mol C)$^{-1}$.

340   *2.3.3 Respiration*

341   The ratio of respiration to secondary production, expressed as energy fluxes, was derived

342   from an empirical relationship between benthic macrofauna biomass and respiration in the Bay-

343   of-Fundy study referenced earlier (Schwinghamer et al., 1986):

344    $$\log_{10}\left(\frac{R}{1\ \text{kcal m}^{-2}\ \text{yr}^{-1}}\right) = \alpha_0 + s \log_{10}\left(\frac{S}{1\ \text{kcal m}^{-2}\ \text{yr}^{-1}}\right)$$ (10)

345   where $s = 0.993$ and $\alpha_0 = 0.367$. Since s is nearly 1, the relationship simplifies to:

346    $R = 10^{\alpha_0} S = 2.33 S$ (11)

347   Assuming that the conversion between carbon and energy is the same for S and R, this equation

348   can be directly applied to these processes expressed as carbon fluxes, consistent with our other

349   carbon flux estimates. Further, combining the relationships of calcification and respiration with

350 secondary production on a molar basis allows a best estimate of the molar ratio of respiration to

351 calcification: $2.33/1.5 = 1.55$.

352 *2.3.4 Impact on the carbonate system*

353 From the estimated benthic macrofaunal calcification (C) and respiration (R), we

354 calculated TA and DIC fluxes (units of mol m^{-2} yr^{-1}):

355 $$F_{TA} = \frac{-2C}{M_{CaCO_3}}$$ (12)

356 $$F_{DIC} = \frac{R}{M_C} - \frac{C}{M_{CaCO_3}}$$ (13)

357 where M_{CaCO_3} and M_C are the molar masses of CaCO$_3$ and C, respectively, and the sign

358 convention is positive from the benthic fauna to the water column. Both calcification and

359 respiration will lead to increases in the concentration of aqueous CO$_2$, and so there is a CO$_2$ flux

360 from benthic fauna that can be decomposed into CO$_2$ fluxes resulting from these two processes:

361 $$F_{CO_2} = F_{CO_2}^{TA} + F_{CO_2}^{DIC}$$ (14)

362 It has been estimated, assuming air–sea CO$_2$ equilibrium, that every mole of CaCO$_3$ precipitated

363 leads to the evasion of 0.6–1 mole of CO$_2$ to the atmosphere, depending on the temperature,

364 salinity, atmospheric pCO$_2$, and initial alkalinity (Chauvaud et al., 2003; Frankignoulle et al.,

365 1998; Ware et al., 1992).

366 In light of strong departures from air–sea CO$_2$ equilibrium in estuaries, including the

367 Chesapeake Bay (Herrmann et al., 2020), we instead estimate the production rate of CO$_2$ using

368 buffer factors, ζ_{TA} and ζ_{DIC}, which are defined as the fractional change in [CO$_2$] divided by the

369 fractional change in [TA] and [DIC], respectively; e.g., $\zeta_{TA} = (\Delta[CO_2]/[CO_2])/(\Delta[TA]/[TA])$.

370 This approach also allows us to estimate the CO$_2$ flux from respiration. We computed the buffer

371 factors in three steps. First, we used output from ROMS-ECB (described in more detail later in

372 the Methods Section 2.4) for the years 1995–2022 and calculated long-term averages of bottom

373 [TA], [DIC], temperature, salinity, and pressure (estimated from water depth) at each model grid

374 cell. These values were used as input to PyCO2SYS (Humphreys et al., 2022) to calculate the

375 baseline [CO₂]. Second, we individually perturbed [TA] and [DIC] by 1% (Δ[TA] and Δ[DIC])

376 while holding all other variables constant and recalculated [CO₂] to get Δ[CO₂]. Third, we

377 computed ζ_{TA} and ζ_{DIC} using the definition of the buffer factors.

378   To relate the fluxes to the buffer factors, we use the flux form of the buffer factors:

379 $$\zeta_{TA} = \frac{F_{CO_2}^{TA}/[CO_2]}{F_{TA}/[TA]} \qquad (15)$$

380 $$\zeta_{DIC} = \frac{F_{CO_2}^{DIC}/[CO_2]}{F_{DIC}/[DIC]} \qquad (16)$$

381 These flux forms take the definitions of the buffer factors and replace ratios of concentration

382 changes (e.g., Δ[CO₂]/Δ[TA]) with ratios of fluxes (e.g., $F_{CO_2}/F_{CO_2}^{TA}$). Using Equations 15 and 16

383 in Equation 14 yields an expression for the CO₂ flux from benthic fauna to the water column:

384 $$F_{CO_2} = [CO_2]\left(\frac{\zeta_{TA}F_{TA}}{[TA]} + \frac{\zeta_{DIC}F_{DIC}}{[DIC]}\right). \qquad (17)$$

385 *2.3.5 Spatial analysis and comparison to other carbon fluxes*

386   To place benthic macrofauna contributions to estuarine carbon cycling in a broader

387 spatial context, we averaged fluxes over 10 regions based on aggregated Chesapeake Bay

388 Program segments (Fig. 1): the major tidal tributaries (the Patuxent, Potomac, Rappahannock,

389 York, and James River Estuaries), the Western and Eastern Shores, and the Upper, Mid, and

390 Lower (mainstem) Bay. Additionally, we computed averages over the mainstem Bay and the

391 whole Bay. For each region, we calculated benthic respiration and bivalve calcification rates

392 based on observed biomass, using the empirically derived equations just described. We then

393   compared these fluxes to other components of the estuarine carbon budget using published

394   values for primary production, allochthonous organic carbon inputs, oyster calcification, and air–

395   sea gas exchange.

396   First, we assessed the extent to which benthic macrofauna remineralize organic carbon

397   inputs by comparing our calculated respiration rates to net primary production (NPP) and

398   external particulate organic carbon (POC) loads. Primary production and POC values were

399   obtained from prior studies (Herrmann et al., 2015; Kemp et al., 1997; Najjar et al., 2018; Zhang

400   & Blomquist, 2018) and scaled to match the spatial extent of our biomass data. In the Upper Bay,

401   we calculated organic carbon inputs by distributing the Susquehanna River's POC load over the

402   combined surface area of the oligohaline and tidal fresh segments (CB1 and CB2, (Olson, 2012).

403   This approach assumes that the majority of the annual POC load from the Susquehanna River

404   remains concentrated in the Upper Bay and is respired rather than transported downstream, an

405   assumption supported by Canuel & Hardison (2016). For comparison, we also distributed

406   Susquehanna River POC inputs across the entire mainstem. For brevity, we restricted our

407   tributary-level comparison to the Potomac River Estuary, where the full organic carbon load was

408   distributed across the surface area of the entire tidal tributary (Fig. 1).

409   Second, we compared our soft-sediment bivalve calcification estimates to published

410   oyster calcification rates from (Fulford et al., 2007). Oyster ash-free dry weight was converted to

411   live weight using a 10:1 ratio (Mo & Neilson, 1994), and a calcification rate of 2 mg $CaCO_3$ per

412   g live weight per day was applied (Waldbusser et al., 2013). Because Eastern oyster (*Crassostrea*

413   *virginica*) populations in the Chesapeake Bay were historically at least two orders of magnitude

414   higher than current levels (Fulford et al., 2007; Newell, 1988), we also scaled published oyster

415   calcification rates up by a factor of 100 to estimate potential historical contributions. This

416 comparison allowed us to place present-day bivalve calcification into the broader context of

417 ecosystem function.

418   Third, we evaluated whether riverine calcium supply could limit observed calcification

419 by estimating annual calcium fluxes from the Susquehanna and Potomac Rivers using non-tidal

420 USGS data from 1995 to 2022 and the Weighted Regression on Time, Discharge, and Season

421 (WRTDS) method (Hirsch et al., 2010). Assuming a 1:1 molar ratio between Ca^{2+} and $CaCO_3$

422 formation, we estimated the maximum potential calcification that could occur if all incoming

423 calcium were used for shell production in adjacent estuarine zones.

424   Finally, we compared CO_2 generated from respiration and calcification (Equation 17) to

425 published estimates of air–sea CO_2 exchange (Chen et al., 2013; Herrmann et al., 2020).

426   The estimated carbon fluxes reveal important spatial patterns, but their interpretation

427 should be tempered by uncertainty in several underlying assumptions. While secondary

428 production models are relatively well-calibrated across estuarine systems, the calculations for

429 calcification and respiration are more sparse and less empirically constrained. Our propagated

430 uncertainty in calcification and respiration incorporates variation in biomass-based carbon

431 content, multiple conversion approaches from biomass to secondary production, and calcification

432 parameters derived from two different bivalve species. Although we used different methods to

433 estimate calcification and propagated these uncertainties accordingly, only one approach was

434 available for respiration.

435   We estimated uncertainties in F_{DIC} and F_{TA}, which represent the propagated uncertainties

436 from respiration and calcification alone, with no additional sources of uncertainty included in

437 those calculations. However, we did not calculate formal uncertainties in F_{CO_2} due to the

438 complexity involved. Additional uncertainty in F_{CO_2} arises from the use of annually averaged,

439 model-derived values for salinity, temperature, depth, DIC, and TA. Further uncertainty stems

440 from the method used to calculate ζ from TA and DIC perturbations. While these additional

441 sources contribute to the overall uncertainty in F_{CO_2}, the uncertainties in F_{DIC} and F_{TA} are likely

442 to remain the dominant contributors.

443   The resulting error bars in the various carbon fluxes reflect these methodological

444 uncertainties, offering a plausible range rather than precise values. Thus, the benthic macrofaunal

445 carbon fluxes presented here should be interpreted with some caution, with more confidence

446 given to the broad spatial patterns and less to the absolute values.

447 *2.4 Environmental predictors of benthic biomass*

448   From the BMP, we used bottom temperature, salinity, and dissolved oxygen data, which

449 are measured with a YSI 660 Sonde or Hydrolab DataSonde 4a in Maryland and a YSI 85 Model

450 meter in Virginia 1 m above the sediment surface. Extreme outliers, defined as data points that

451 fall beyond three times the interquartile range from the first or third quartile, were removed. As a

452 result, one value for dissolved oxygen and one for water temperature were excluded from the

453 analysis. The salinity zones are also characterized at each site as tidal fresh (<0.5 ppt),

454 oligohaline (0.5–5 ppt), low mesohaline (5–12 ppt), high mesohaline (12–18 ppt), and polyhaline

455 (>18 ppt); these zones are relatively geographically fixed (with some changes in 2011 due to

456 Hurricane Irene and Tropical Storm Lee) based on long-term averages of salinity (Llansó, 2002;

457 Llansó & Zaveta, 2017). Sediment sand fraction was measured by first collecting two 120 ml

458 benthic grab sub-samples. Sand particles are separated by wet-sieving through a 63-μm stainless

459 steel sieve. Sand fraction is recorded after drying and weighing the samples. The bottom water

460 quality and sediment composition data were time-averaged using the same scheme described

461 earlier for the benthic biomass data.

462   ROMS-ECB output was used to characterize environmental variables not measured by

463   the BMP that could be relevant to predicting the benthic macrofauna biomass distribution.

464   ROMS-ECB uses 20 terrain-following vertical levels and a uniform horizontal resolution of 600

465   m (St-Laurent & Friedrichs, 2024b). We compiled daily averaged output at various grid points

466   from 1995 to 2022 corresponding to the locations of each of the 8128 benthic biomass samples.

467   We selected the ROMS output at the nearest ROMS grid point to each BMP sample location for

468   each variable of interest, described below. Several ROMS-ECB environmental variables are

469   directly linked to primary production, but the timing of peak primary production does not always

470   align with periods of greatest food availability for benthic organisms. To capture ecologically

471   meaningful variation in benthic–pelagic coupling, we calculated both seasonal and annual

472   averages for each variable. Seasonal groupings reflect key ecological periods: spring (March–

473   May), which includes the diatom bloom that delivers fresh organic material to the benthos, and

474   summer (June–August), characterized by stratification, hypoxia, and intense remineralization.

475   Fall (September–November) and winter (December–February) were also included to represent

476   background seasonal variability. We then time-averaged the seasonal and annual means as

477   described earlier. Coverage dropped from 868 to 846 cells after adding ROMS-ECB outputs,

478   largely where the model masks shallow/tributary cells or lacks complete seasonal data.

479   We used ROMS-ECB output, as opposed to data from the Chesapeake Bay Water Quality

480   Monitoring Program (WQMP), which has measured water quality variables since 1984 at over

481   100 tidal stations (Chesapeake Bay Program, n.d.). However, the stations are at different

482   locations than the BMP stations, requiring interpolation to correlate these data with benthic

483   biomass. Other studies have opted to use kriging, a method used to spatially interpolate surface

484   water quality data, to increase the spatial resolution. Kriging has been found to outperform the

485 standard inverse distance weighting tools typically used in the Chesapeake Bay (Murphy et al.,

486 2015). One study evaluated the kriging of surface WQMP data for July 2007 using 117–123 data

487 points (Murphy et al., 2015). In cross-validation, one measured sample is removed, and the

488 interpolation is then performed at that location; the interpolated value is then compared to the

489 observed value. Cross-validation of temperature, salinity, and dissolved oxygen yielded root-

490 mean-square errors (RMSE) of 0.75 °C, 1.1 ppt, and 1.2 mg L^{-1}, respectively. In contrast,

491 ROMS-ECB output was evaluated with over 500,000 WQMP data points at multiple depths and

492 locations from 1985 to 2021 (St-Laurent & Friedrichs, 2024a). The RMSEs for temperature,

493 salinity, and dissolved oxygen were 1 °C, 1.9 psu, and 1.5 mg L^{-1}, respectively. Although these

494 RMSEs are slightly higher than those from kriging, the evaluation was much more robust, and

495 the long time series evaluation is more relevant to our time-averaging technique over 28 years. In

496 addition, we wanted to utilize bottom water quality data, as these variables are measured closer

497 to the location of benthic macrofauna. However, cross-validation for kriging was only performed

498 at the surface (Murphy et al., 2015), possibly due to the challenges of accounting for bottom

499 topography in spatial interpolation.

500   ROMS-ECB simulates many variables, and we considered the subset that might be good

501 predictors of benthic biomass: bottom POC, bottom total suspended solids (TSS), and surface

502 NO_3^-. POC was considered because a large fraction of POC represents food for benthic

503 macrofauna. TSS was considered a metric of suspended inorganic material, which can inhibit

504 filter-feeding organisms (Grant & Thorpe, 1991). Photosynthesis is largely limited by NO_3^- in

505 the Chesapeake Bay (Zhang et al., 2021); because phytoplankton productivity and the subsequent

506 sinking of POC is an important source of organic matter to the benthos, NO_3^- could be a

507 predictor of benthic biomass. ROMS-ECB output was evaluated for robustness with WQMP data

508   using Spearman's rank correlation coefficient, R_s, which measures the strength of the association

509   between two variables (Hauke & Kossowski, 2011). In our analysis of benthic biomass

510   predictors, we included only variables with R_s above 0.7, which generally indicates a strong

511   association (Akoglu, 2018). NO_3^- was used as it had $R_s = 0.77$, whereas POC and TSS were not

512   as they had $R_s = 0.26$ and 0.24, respectively (St-Laurent & Friedrichs, 2024a).

513   We also considered potentially good predictors that could be computed from ROMS-

514   ECB output: surface oxygen supersaturation (ΔO_2) and bottom aragonite saturation state (Ω_{arag}).

515   ΔO_2 can be used as a tracer for net ecosystem production (Herrmann et al., 2020) and hence may

516   indicate organic matter availability to the benthos. $\Delta[O_2]$ is equal to O_2 minus the saturation

517   concentration, which was computed from temperature and salinity (Garcia & Gordon, 1992).

518   Positive ΔO_2 values are favored during net autotrophy (photosynthesis exceeds respiration),

519   while negative values are favored during net heterotrophy (respiration exceeds photosynthesis);

520   temperature change and transport can also create non-zero ΔO_2. Ω_{arag} could predict benthic

521   biomass because bivalve calcification is expected to depend on this metric (Thomsen et al.,

522   2015). PyCO2SYS (Humphreys et al., 2022) was used to derive the solubility product and

523   carbonate ion concentration from alkalinity, DIC, temperature, salinity, and water depth. We

524   examined ΔO_2 and Ω_{arag} in the subsequent statistical analysis because the ROMS-ECB output

525   variables used to compute them all had $R_s > 0.7$. Although calcium measurements were not

526   available for model evaluation, it is highly correlated to salinity, though deviations may occur at

527   low salinity (Beckwith et al., 2019).

528   *2.5 Statistical modeling of benthic biomass*

529   We used GAMs to evaluate how bottom water quality and biogeochemical model outputs

530   predict the spatial distribution of benthic macrofaunal biomass. GAMs are data-driven statistical

531   models that have been widely applied in coastal ecology since the late 20th century (Guisan et

532   al., 2002; Smith et al., 2023). They model additive, smoothed relationships between predictor

533   and response variables, making them well-suited for capturing the non-linear, non-monotonic

534   patterns often observed in ecological datasets (Grüss et al., 2014; Guisan et al., 2002; Hastie &

535   Tibshirani, 1987; Wood, 2017). GAMs also quantify the strength and relative contribution of

536   each predictor (Guisan et al., 2002) and have demonstrated predictive performance comparable

537   to or exceeding other modeling approaches (Drexler & Ainsworth, 2013). We used the mgcv

538   package in R and applied restricted maximum likelihood (REML) to optimize smoothness

539   (Wood, 2011; Wood, 2017). This approach is particularly effective with large datasets like ours,

540   enabling robust estimation of spatial patterns in biomass across a broad geographic region (Grüss

541   et al., 2014; Wood, 2011). Although GAMs can handle non-normal distributions of the response

542   variable (Guisan et al., 2002), we found the best model fit by applying a natural logarithmic

543   transformation to the biomass. A small constant (0.0001 g m^{-2}) was added to the biomass values

544   before applying the natural logarithmic transformation to account for zeros in the data.

545   As described earlier, we initially identified eight environmental variables: O_2, salinity,

546   total depth, water temperature, sand fraction, NO_3^-, Ω_{arag}, and $\Delta[O_2]$. To avoid multicollinearity,

547   which can distort GAM results (Grüss et al., 2014; Grüss et al., 2018; Guisan et al., 2002), we

548   used Pearson's correlation coefficients (r) to evaluate the linear correlation between the predictor

549   variables. When two variables were highly correlated ($r > 0.7$) (Dormann et al., 2013), we

550   retained the variable that was more directly measurable and broadly understood across estuarine

551   systems. Based on this assessment, we excluded Ω_{arag} and $\Delta[O_2]$ due to their strong correlation

552   with other variables and retained the remaining six variables for GAM analysis. While necessary

553   for model stability, this approach may limit the explanatory power of the GAM by excluding

554 ecologically meaningful predictors. The full list of candidate variables and their inclusion status

555 is provided in Table 1.

556 Table 1: Predictor variables from the Chesapeake Bay Benthic Monitoring Program and ROMS-

557 ECB compiled from 1995–2002. For ROMS-ECB output, daily values were used to calculate

558 annual averages and seasonal averages for spring (March–April), summer (July–August), fall

559 (September–November), and winter (December–February)

Dataset	Location	Variable	Units	Processing	Used in GAMs?
BMP	Bottom	O_2	mmol m^{-3}	Removed extreme outliers	Yes
BMP	Bottom	Salinity	ppt	None	Yes
BMP	Bottom	Total depth	m	None	Yes
BMP	Bottom	Water temperature	°C	Removed extreme outliers	Yes
BMP	Bottom	Sand fraction	%	None	Yes
ROMS-ECB	Surface	NO_3^-	mmol m^{-3}	Annually and seasonally averaged	Yes
ROMS-ECB	Bottom	POC	mmol m^{-3}	Annually and seasonally averaged	No, model evaluation gave poor results

ROMS-ECB	Bottom	TSS	mg L^{-1}	Annually and seasonally averaged	No, model evaluation gave poor results
ROMS-ECB	Bottom	Ω_{arag}		Calculated from alkalinity, DIC, temperature, water depth, and salinity using PyCO2SYS. Annually and seasonally averaged	No, highly correlated with salinity
ROMS-ECB	Surface	$\Delta[O_2]$	mmol m^{-3}	Calculated from oxygen, salinity and temperature using Gracia & Gordon (1991, 1992). Annually and seasonally averaged	No, highly correlated with salinity and NO$_3^-$

560   We used Akaike's Information Criterion (AIC), a statistical measure that has been

561 increasingly used in ecology, to evaluate which combination of parameters results in the best

562 model fit (Symonds & Moussalli, 2011). AIC is calculated using the number of fitted parameters

563 in the model, the maximum likelihood estimate, and the residual sum of squares (Symonds &

564 Moussalli, 2011). Among the candidate models, the one with the lowest AIC value offers the

565 best balance between explanatory power and simplicity, requiring the fewest necessary

566   parameters. We chose the assemblage of predictor variables in our model that minimized AIC.

567   We generally used annually averaged predictor variables from the ROMS-ECB output because

568   using seasonal averages had a negligible difference on the AIC. To assess the relative influence

569   of each predictor variable, we used Akaike weights, which indicate the probability that a given

570   model is the best among those considered. We ranked models by AIC and summed the Akaike

571   weights for all models containing each predictor variable. Higher Akaike weights indicate

572   stronger support for a variable's inclusion in the best-fitting models. Interaction terms between

573   predictor variables were examined, but their inclusion did not significantly improve the AIC

574   values.

575   **3. Results**

576   ***3.1 Spatial distribution of benthic macrofauna biomass***

577   The time-averaged (1995–2022) summer benthic macrofauna biomass exhibits strong

578   spatial variability across the Chesapeake Bay, with higher concentrations in the tidal fresh and

579   oligohaline zones, and lower concentrations in the Mid Bay and lower sections of many

580   tributaries (Figure 2, 3a). The arithmetic mean of all biomass measurements based on the full

581   data set, $N = 8128$ is 7.93 g m^{-2} (median = 0.98 g m^{-2}), whereas the spatial mean across all grid

582   cells with at least one biomass measurement ($N = 1295$) is 7.16 g m^{-2} (median = 1.39 g m^{-2}). The

583   sampling scheme oversamples the tidal tributaries (Fig. A1), where biomass density is higher,

584   inflating the arithmetic mean. The standard deviation of the full dataset is 28.7 g m^{-2}, indicating

585   that the distribution is heavily skewed to the right, with the highest sample reaching up to 722 g

586   m^{-2}. The standard deviation of the time-averaged data is 18.0 g m^{-2}, considerably smaller than

587   the full data set since it does not include temporal variability, but is nevertheless still skewed to

588   the right, with the highest gridded value of 220 g m^{-2}. Most of the high-biomass density zones

589 (>30 g m^{-2}) are concentrated in the tidal fresh and oligohaline sections of the mainstem and

590 Potomac River Estuary. The other tributaries have higher biomass in the tidal fresh and

591 oligohaline and zones compared to the other salinity zones. In the Mid Bay and lower sections of

592 many tributaries, biomass is very low.
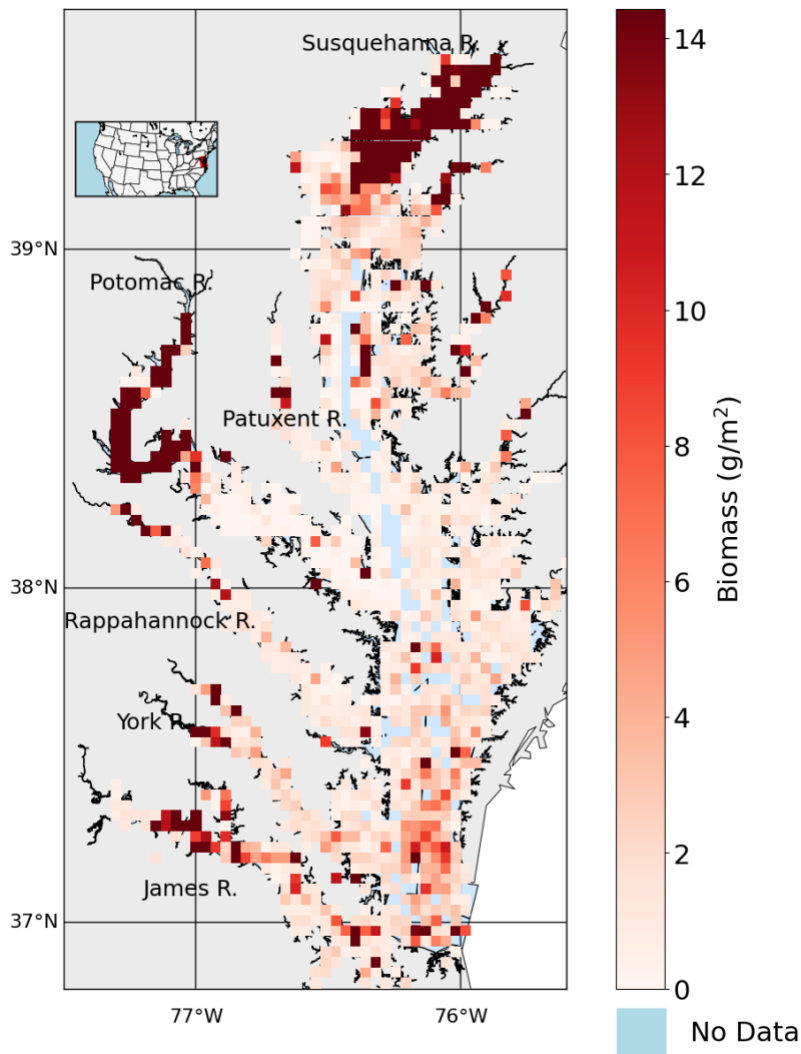
593

594 Figure 2: Average summer biomass density from 1995 to 2022 from the Chesapeake Bay

595 Benthic Monitoring Program. Biomass values are shown using a red color scale, white represents

596 0 g m^{-2}, light blue indicates open water grid cells with no data, and gray represents land areas

597 with no data.

598   The distribution of the biomass into salinity zones for multiple taxonomic groups and

599   species is shown in Fig. 3b–f. Bivalves dominate biomass in all salinity zones, except the

600   polyhaline, where they are comparable to polychaetes. Bivalves comprise 88.0% of the benthic

601   biomass, and polychaetes comprise 7.3%. At a taxonomic species level, the bivalve *R. cuneata*

602   comprises 66.1% of the biomass, followed by the bivalves *C. fluminea* (8.0%) and *L. balthica*

603   (7.5%). Appendix D provides a more detailed spatial analysis of species distribution. The high-

604   biomass zones in the Upper Bay, Potomac River Estuary, and James River Estuary are

605   dominated by *R. cuneata*, mostly in the oligohaline zone (Figs. 3c & D1). *C. fluminea* also

606   dominates in relatively higher quantities in the tidal fresh zone of the Potomac River Estuary and

607   the tidal fresh zone of the Upper Bay (Figs. 3d & D1). In general, *R. cuneata* has a higher

608   biomass density in the tidal fresh than *C. fluminea* because *R. cuneata* is present in all tidal fresh

609   zones. *L. balthica* is distributed in multiple salinity zones; it is highest in the lower mesohaline

610   and is the dominant species in the lower mesohaline zone of the Upper Bay and Patuxent River

611   Estuary (Figs. 3e & D1). The biomass density of *L. balthica* in the lower mesohaline (<2 g m^{-2})

612   is significantly lower than that of *C. fluminea* and *R. cuneata* in the tidal fresh and oligohaline

613   zones. Polychaetes are the species that dominate over the largest geographic area, throughout the

614   polyhaline and part of the higher mesohaline (Figs. 2, 3f, & D1). However, their biomass density

615   is low relative to bivalves (<2 g m^{-2}). Bivalves are sparse throughout the higher mesohaline and

616   polyhaline zones.
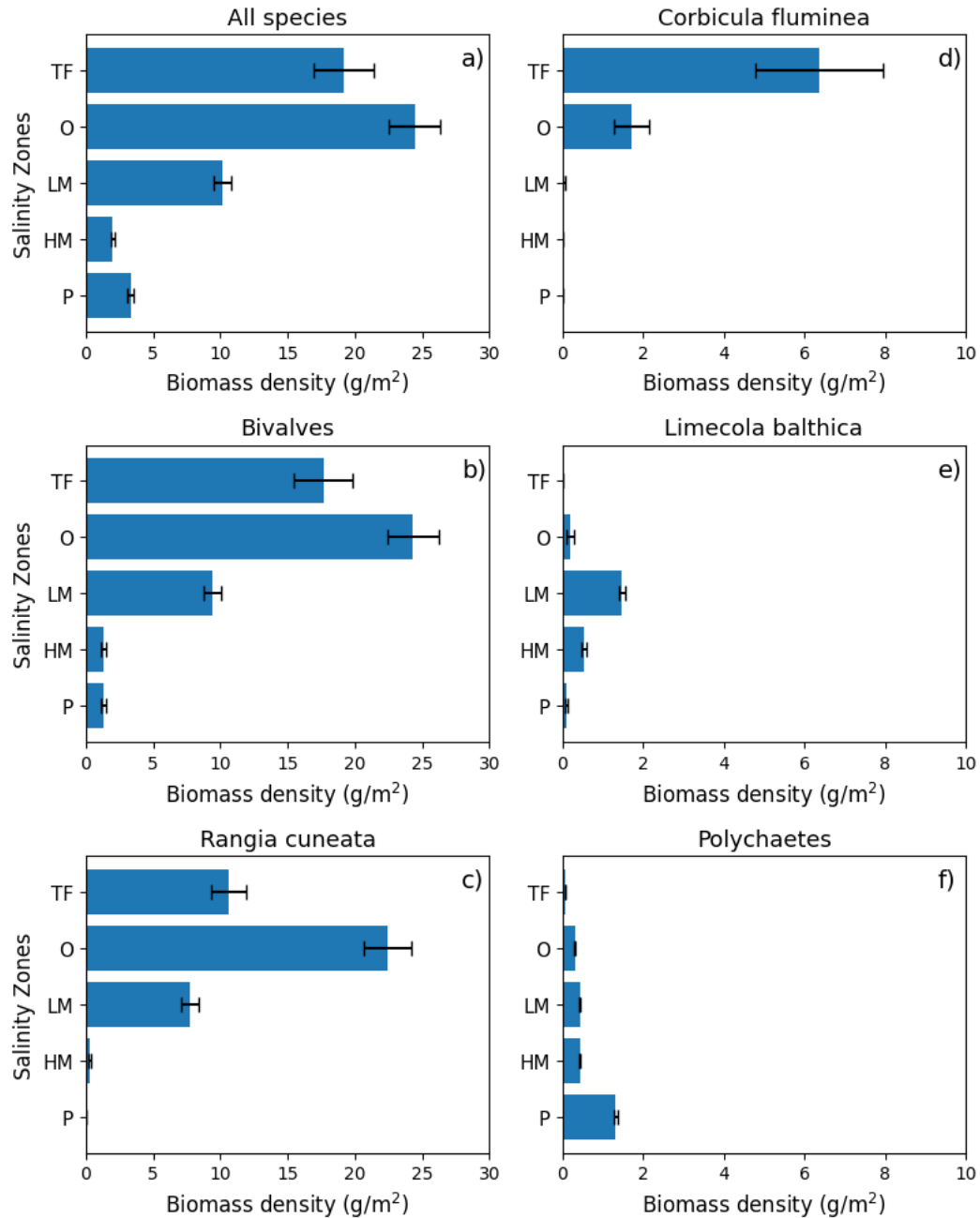
Figure 3: Average summer benthic biomass density of multiple classes and species in each salinity zone from 1995 to 2022. The salinity zones are determined by the BMP based on the long-term average of salinity in each geographic zone: TF – Tidal Freshwater (0–0.5 ppt), O – Oligohaline (0.5–5 ppt), LM – Low Mesohaline (5–12 ppt), HM – High Mesohaline (12–18 ppt), and P – Polyhaline (≥18 ppt). Averages and standard errors (bars) are computed using the full

623   data set, not the gridded values. Note the difference in horizontal scale between the left and right

624   columns.

3.2 Carbon flux estimates

626   Average benthic macrofaunal carbon and alkalinity fluxes vary across the 10 regions of

627   the Bay (Fig. 4). Among the different fluxes, which are all presented on a molar basis in Figure

628   4, F_{TA} has the largest magnitude, followed, in decreasing order, by F_{CO_2}, respiration (R/M_C),

629   calcification (C/M_{CaCO3}), and F_{DIC}. We first discuss calcification, respiration, F_{TA}, and F_{DIC}.

630   Calcification is 1.55 times respiration (best estimate), as a result of the molar ratio of these

631   processes (Section 2.3.3). F_{TA} is always negative, as expected because calcification is an

632   alkalinity sink, and twice the magnitude of calcification (Equation 12). The best estimate of F_{DIC}

633   was mostly positive, though it could be positive or negative because calcification is a DIC sink

634   and respiration is a DIC source (Equation 13). The best estimate of F_{DIC} ends up being positive

635   because respiration exceeds calcification. Using the best estimate of the molar

636   respiration:calcification ratio (1.55) and Equations 12 and 13, it can be shown that $-F_{TA}/F_{DIC} =$

637   3.6, consistent with the results in Fig. 4. Estimated uncertainties (Appendix B) were

638   approximately 45% for calcification, 40% for respiration, 135% for F_{DIC}, and 45% for F_{TA}. The

639   uncertainty for F_{DIC} being greater than 100% admits the possibility of negative DIC fluxes.

640   F_{CO_2} is always positive because benthic macrofauna remove TA from and add DIC to the

641   water column. The magnitude of F_{CO_2} can be understood by first noting that it is proportional to

642   F_{TA} and F_{DIC}, with proportionality constants of $[CO_2]\zeta_{TA}/[TA]$ and $[CO_2]\zeta_{DIC}/[DIC]$,

643   respectively (Equation 17; note that $F_{TA} < 0$ and $\zeta_{TA} < 0$, leading to $F_{CO_2} > 0$). In the open ocean,

644   using mean conditions of $pCO_2 = 400$ µatm, $[TA] = 2300$ µmol kg^{-1}, temperature = 15 °C, and

645   salinity = 35, we can use carbonate system equilibria to estimate $[CO_2] \sim 15$ µmol kg^{-1}, $[DIC] \sim$

646   2100 µmol kg^{-1}, and $-\zeta_{TA} \sim \zeta_{DIC} = 11$, which leads to F_{CO_2} about 7–8% of $-F_{TA}$ and F_{DIC}. Here,

647   we are seeing F_{CO_2} comparable in magnitude to F_{TA} and F_{DIC} because Bay waters tend to have

648   higher [CO_2] and ζ_{DIC} and lower [TA] and [DIC] than what is observed in open-ocean waters, as

649   we show in Appendix E and Fig. E1. We observe much larger F_{CO_2} in tidal fresh (6–18 mol m^{-2}

650   yr^{-1}) compared to oligohaline (3–7 mol m^{-2} yr^{-1}) waters (Fig. 4), despite comparable values of

651   F_{DIC} and F_{TA}. These differences in F_{CO_2} between tidal zones are primarily driven by [CO_2],

652   which is much higher in the tidal fresh due to a lower TA:DIC ratio (Fig. E1l). The magnitudes

653   of the buffer factors are also greater in lower salinity waters (Figs. E1g & E1h), decreasing

654   slightly in the polyhaline. Polyhaline values (13–16) are comparable to oceanic estimates of 9–15

655   (Egleston et al., 2010).

656
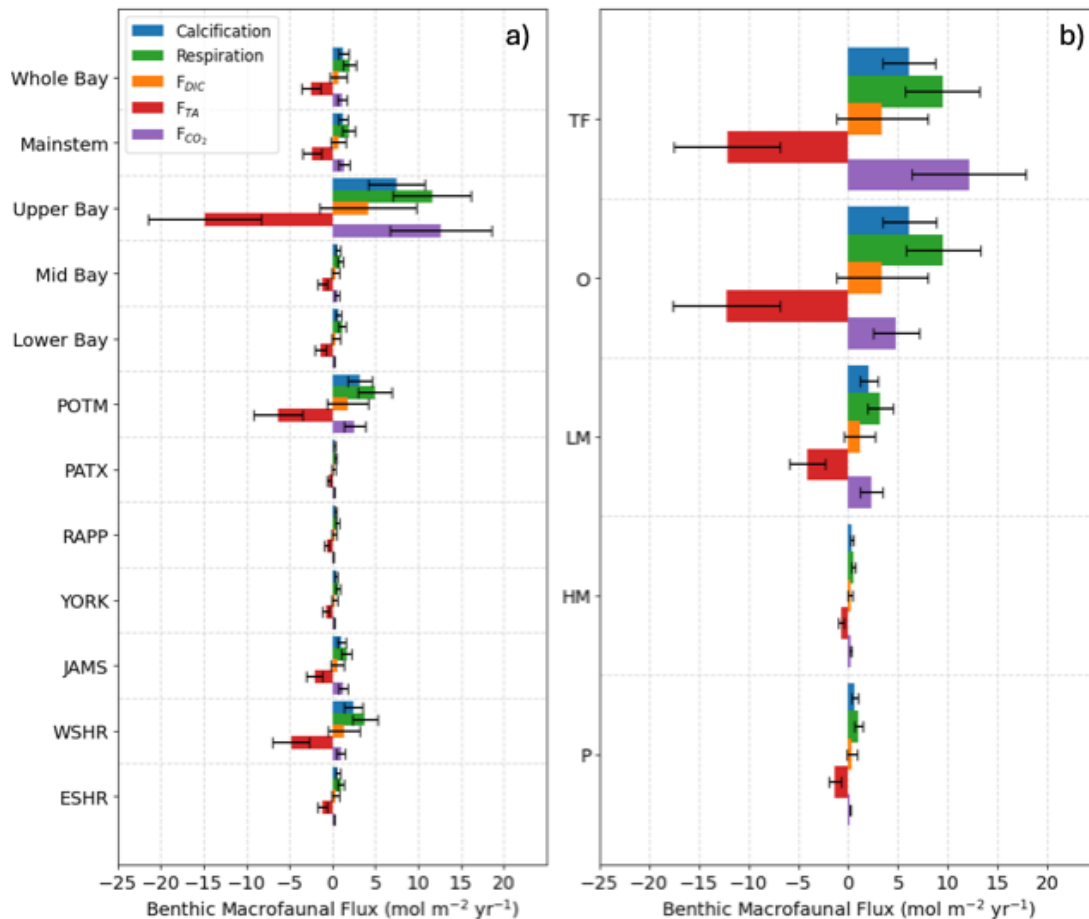
657   Figure 4: Average benthic macrofaunal fluxes by (a) Bay region and (b) salinity zone. Tributary

658   and sub-estuarine acronyms: ESHR – Eastern Shore tributaries; WSHR – Western Shore

659   tributaries; POTM – Potomac River; PATX – Patuxent River; RAPP – Rappahannock River;

660   YORK – York River system (including Mattaponi and Pamunkey Rivers); JAMS – James River.

661   Salinity zone abbreviations: TF – Tidal Freshwater (0–0.5 ppt), O – Oligohaline (0.5–5 ppt), LM

662   – Low Mesohaline (5–12 ppt), HM – High Mesohaline (12–18 ppt), P – Polyhaline (≥18 ppt).

663   Error bars represent uncertainty ranges (Appendix B).

664   In multiple segments of the Bay, benthic macrofaunal respiration rates (R) are

665   comparable to the total available organic carbon supply, defined here as the sum of net primary

666   production (NPP) and riverine POC loads (Table 2). In the Upper Bay, benthic macrofaunal

667   respiration rates are within the range of NPP alone. When combined with POC loads, our

668   estimates suggest that benthic macrofauna respire approximately f = 18–45% of the total

669   available organic carbon, where:

670
$$f = \frac{R}{NPP + POC} \tag{18}$$

671
$$\frac{\Delta f}{f} = \sqrt{\left(\frac{\Delta R}{R}\right)^2 + \left(\frac{\Delta NPP}{NPP}\right)^2} \tag{19}$$

672   Here, ΔR and ΔNPP are the standard errors of R and NPP, respectively. This formulation is

673   consistent with the uncertainty propagation approach described in Appendix B.

674   In the Potomac River Estuary, respiration rates exceed external organic carbon loads,

675   although NPP estimates for this region were unavailable. By contrast, in the mainstem and across

676   the Bay as a whole, benthic respiration rates are much smaller than NPP, accounting for only 3–

677   8% of the total inputs of organic carbon to the mainstem. These percentages were calculated

678   using the same approach as in Equations 18–19, but substituting mainstem benthic macrofaunal

679   respiration, NPP, and POC inputs.

680   Table 2: Riverine POC load, net primary production (NPP), and benthic respiration compiled

681   from the listed studies compared with benthic macrofaunal respiration from our study. POC load

682   estimates from Zhang & Blomquist (2018) were based on USGS river monitoring data combined

683   with flow-weighted sediment and organic carbon concentrations. For POC loads we specifically

684   used values from Table S5 of Zhang & Blomquist (2018), which reports long-term average true-

685   condition annual loads. Susquehanna loads were distributed across the mainstem and Upper Bay,

686   Potomac River loads were distributed across the Potomac, and total watershed load was

687   distributed across the whole Bay. These loads were divided by the surface area of the

688   corresponding segment area (Chesapeake Bay Program, 2004) NPP values from Harding et al.

689   (2002) were derived from depth-integrated in situ ^{14}C-uptake incubations across multiple cruises,

690   scaled using statistical models. Benthic respiration values from Kemp et al. (1997) were

691   estimated by combining seasonal in situ measurements of sediment oxygen consumption with

692   sulfate reduction rates, together accounting for microbial and macrofaunal respiration.

Region	Carbon Flux	Value (g C m^{-2} yr^{-1})	Reference
Whole Bay	Riverine POC load	12.0	Zhang & Blomquist (2018)
	Benthic macrofaunal respiration	24 ± 9	This study
Mainstem	Riverine POC load	18.8	Zhang & Blomquist (2018)
	NPP	385 ± 17	Harding et al. (2002)
	Benthic respiration	163.1	Kemp et al. (1997)
	Benthic macrofaunal respiration	22 ± 9	This study
Upper Bay	Riverine POC load	257.7	Zhang & Blomquist (2018)
	NPP	182 ± 27	Harding et al. (2002)
	Benthic respiration	44.3	Kemp et al. (1997)
	Benthic macrofaunal respiration	139 ± 55	This study

Potomac	Riverine POC load	31.9	Zhang & Blomquist (2018)
	Benthic macrofaunal respiration	59 ± 24	This study

693   Benthic macrofauna also contribute substantially to the calcium budget of the Bay. We

694   estimate that calcification by benthic macrofauna monitored in the BMP is slightly lower than

695   historical (pre-decline) estimates of the Eastern oyster (*Crassostrea virginica*) calcification in the

696   mainstem Bay but exceeds post-decline estimates by about 7 to 19 times in the Upper Bay (Table

697   3). This range was calculated by taking the upper and lower bounds of our measured calcification

698   rates (mean ± uncertainty) and dividing each by the post-decline oyster calcification rate.

699   Evaluating the role of bivalve calcification in utilizing calcium further underscores its

700   biogeochemical significance. Relative to annual riverine calcium fluxes, benthic macrofauna

701   would use ~22–58% of the available calcium in the Upper Bay and nearly all in the Potomac

702   River. These percentages were likewise calculated by taking the lower and upper bounds of our

703   measured calcification rates (mean ± uncertainty) and dividing each by the corresponding

704   maximum potential riverine calcium input, which was treated as fixed.

705   Table 3: Historic oyster calcification rates and estimated maximum potential calcification based

706   on riverine calcium input, compared with calcification rates from this study. Riverine calcium

707   load from the Susquehanna River was distributed across the Upper Bay and across the mainstem,

708   calcium load from the Potomac River was distributed within the Potomac segment, and the sum

709   of all riverine calcium inputs was distributed across the Whole Bay.

Region	Calcification Rate	Value (g CaCO$_3$ m^{-2} yr^{-1})	Reference
Whole Bay	Riverine Ca load	135	USGS
	Benthic macrofauna	142 ± 62	This study
Mainstem	Riverine Ca load	213	USGS
	Oysters	139	Fulford et al. (2007); Waldbusser et al. (2013)
	Benthic macrofauna	120 ± 54	This study
Upper Bay	Riverine Ca load	1861	USGS

	Oysters	57	Fulford et al. (2007); Waldbusser et al. (2013)
	Benthic macrofauna	747 ± 329	This study
Potomac	Riverine Ca load	262	USGS
	Benthic macrofauna	316 ± 142	This study

The role of benthic macrofaunal metabolic processes in the carbon budget is particularly

pronounced when the effects of calcification and respiration are combined to estimate CO_2

production. This CO_2 flux exceeds the amount of outgassing estimated in the Upper Bay and the

mainstem overall (Table 4).

Table 4: Air–sea gas exchange from the listed studies compared with total benthic macrofaunal

CO_2 flux calculated in our study.

Region	CO₂ Flux	Value (g C m⁻² yr⁻¹)	Reference
Whole Bay	Benthic macrofauna	13 ± 10	This study
Mainstem	Air–sea exchange	14.5 (outgassing)	Herrmann et al. (2020)
	Benthic macrofauna	16 ± 13	This study
Upper Bay (CB1–CB3)[a]	Air–sea exchange	74.5 (outgassing)	Herrmann et al. (2020)
(CB1 & CB2)[a]	Benthic macrofauna	151 ± 121	This study

[a] CB1–CB3 refer to Chesapeake Bay Program segmentation units (Chesapeake Bay Program,

2004): CB1 = tidal fresh, CB2 = oligohaline; CB3 = mesohaline.

3.3 Correlation of environmental variables with biomass

The GAMs analysis, based on gridded, time-averaged biomass data, revealed key drivers

of benthic biomass both at the community level (all taxa combined) and for specific taxonomic

groups and species. The results for total benthic biomass (all taxa), polychaetes, and the bivalve

species *R. cuneata*, *C. fluminea*, and *L. balthica* are shown in Table 5. The bivalve group was

excluded from the table because its results were nearly identical to total benthic biomass results.

For total benthic biomass, the predictor variables (O_2, salinity, total depth, water temperature,

725   sand fraction, and NO_3^-) explain 54.9% of the deviance in biomass. For individual taxa, the

726   predictive capability of GAMs increases, with 73.7% of *R. cuneata* biomass deviance explained

727   by the predictor variables. For total benthic biomass, dissolved oxygen emerged as the strongest

728   predictor (with the highest summed Akaike weight), followed by total depth, salinity, and NO_3^-.

729   Although water temperature and sand fraction were included in the model, they had relatively

730   little influence. For individual taxa, dissolved oxygen became less influential, especially for *R.*

731   *cuneata* and *C. fluminea*. Salinity generally increased in influence as a predictor variable for

732   species-specific models, most notably for *C. fluminea*. NO_3^- also generally increased in influence

733   as a predictor variable for species-specific models, with very high influence as a predictor of *C.*

734   *fluminea* biomass.

735   Table 5: The best-fitting generalized additive model (GAM) for each taxa assemblage,

736   determined by minimizing Akaike's Information Criterion (AIC). $N = 846$ (number of grid boxes

737   with data) for all models. Summed Akaike weights indicate the relative importance of each

738   predictor variable across all models considered, with higher values suggesting stronger support

739   for a variable's inclusion in the best-fitting models. "N/A" indicates that the variable was not

740   included in the best model. Some variables may have high summed Akaike weights even if they

741   are not in the best-fitting model. For example, in the *R. cuneata* model, O_2 has a summed Akaike

742   weight of 0.571, while water temperature has 0.032. In the *C. fluminea* model, O_2 has 0.384, and

743   total depth has 0.24.

Taxa	Deviance Explained	Summed Akaike Weight					
		O_2	Salinity	Total Depth	Water temperature	Sand fraction	NO_3^-
All taxa	54.9%	0.536	0.032	0.400	0.000	0.000	0.031

Polychaetes	50.0%	0.457	0.173	0.266	N/A	0.000	0.104
R. cuneata	73.7%	N/A	0.161	0.183	N/A	0.024	0.059
C. fluminea	65.9%	N/A	0.212	N/A	0.122	0.078	0.132
L. balthica	58.4%	0.888	0.000	0.112	N/A	0.000	0.000

744   The relative effects of O_2, salinity, NO_3^- and total depth on benthic biomass varied

745   considerably, as shown in the partial plots of Figure 5. Macrofauna biomass reaches its lowest

746   values at low dissolved oxygen, the only section of all the partial plots that reach 0 g m^{-2}.

747   Biomass is generally higher at shallower depths, although the effect is small. Biomass is highest

748   at both low and high salinities and high surface NO_3^-. In summary, biomass is highest at

749   moderate dissolved oxygen, shallow depths, low or high salinities, and high NO_3^-.

750
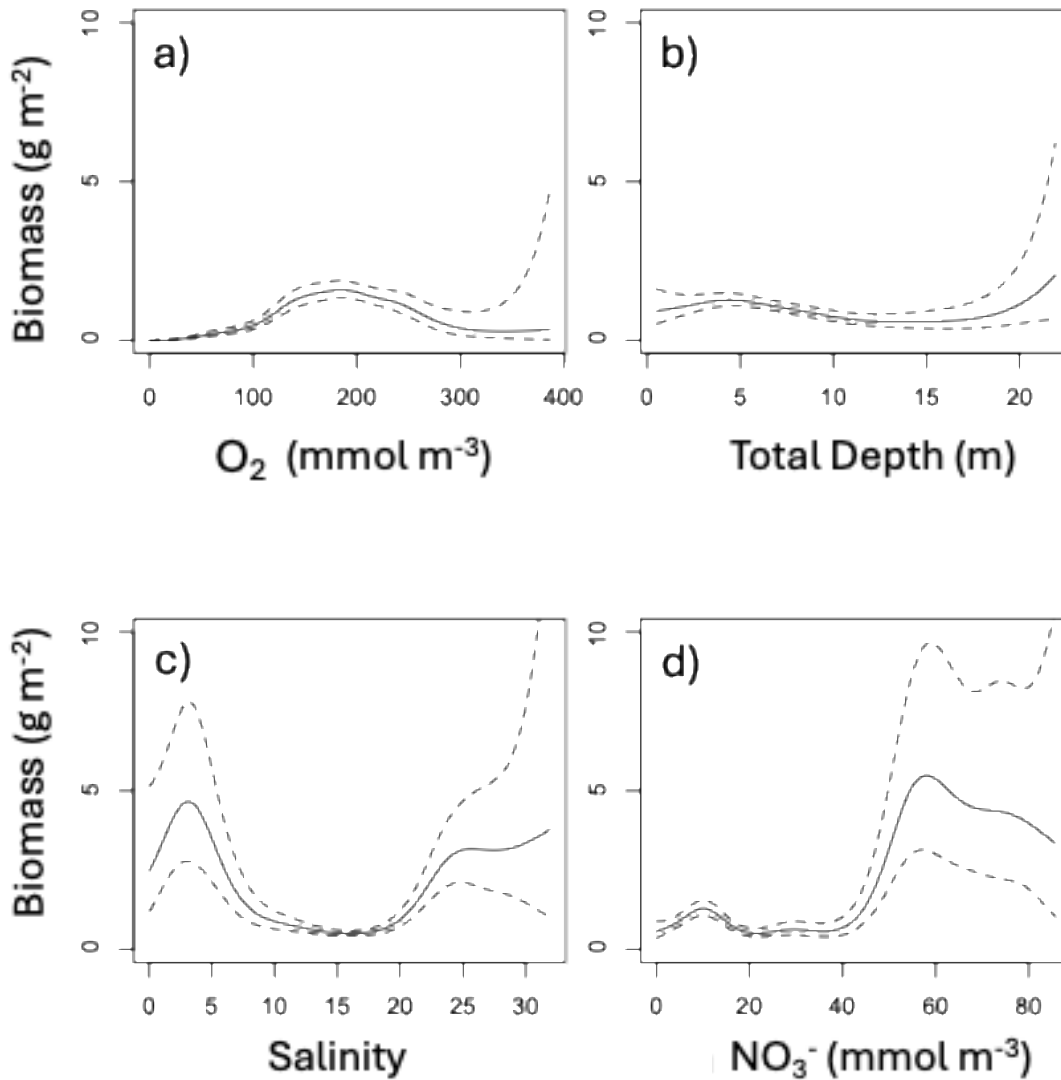
751 Figure 5: Partial plots of the effect of significant predictor variables on total biomass: (a) bottom

752 dissolved oxygen, (b) total depth, (c) bottom salinity, and (d) surface nitrate. Water temperature

753 and sand fraction were included in the model but omitted from display as they did not

754 significantly improve the model fit. The solid black line shows the response and the dashed lines

755 show the 95% confidence interval. The natural log transformation was removed from biomass to

756 enhance viewing of the partial plots. The x-axis was cut off at the upper quartile plus three

757 interquartile ranges in order to remove extreme outliers from the plots.

758   The model fit evaluation, presented in Appendix F and Fig. F1, reveals some systemic

759   biases. The residuals (observed values minus model-fitted values) are slightly skewed to the left

760   (Fig. F1b), meaning the model is more likely to overestimate biomass. The response vs. fitted

761   value scatter plot shows a nearly linear relationship (Fig. F1a). The map of residuals (Fig. F1c)

762   shows that there is also an underestimation in the model fit at the high biomass zones, especially

763   in the Upper Bay.

764   **4. Discussion**

765   *4.1. Benthic macrofaunal contributions to the Chesapeake Bay carbon budget*

766   The higher benthic biomass in less saline waters of the Chesapeake Bay suggests a

767   significant role for respiration in the carbon budget in this region. The proportion of the total

768   input of particulate organic carbon that is respired by benthic macrofauna estimated in our study

769   in the Upper Bay (18–45%) is similar to the 14 to 40% range estimated for bivalve filter feeders

770   in tidal fresh and oligohaline waters by Cerco & Noel (2010). In the Upper Bay, where the

771   benthic macrofauna respiration is comparable to NPP, if all the NPP were respired solely by

772   benthic macrofauna, net ecosystem production would be zero. However, given the consideration

773   of additional respiration by other organisms (e.g., microbes and pelagic zooplankton) the

774   allochthonous POC from the Susquehanna River must be a critical source of organic carbon

775   driving net heterotrophy in this region. These findings reinforce the earlier conclusion that high

776   biomass zones in the Upper Bay are sustained by allochthonous organic inputs. The Potomac

777   River Estuary, however, presents a less conclusive case, partly due to the lack of available NPP

778   estimates. In this estuary, where benthic macrofaunal respiration exceeds the estimated POC

779   flux, additional carbon sources, such as autochthonous NPP or tidal wetland outwelling, may be

780   contributing to carbon metabolism. Notably, Herrmann et al. (2015) estimated that the amount of

781 organic carbon exported through wetland outwelling is approximately equal to half of that

782 exported by streamflow in Mid-Atlantic estuaries, highlighting its potential significance in

783 supporting heterotrophic processes in the Potomac.

784   Benthic macrofaunal respiration plays a smaller role in the rest of the Bay, where

785 autochthonous organic carbon dominates. For both the mainstem and the whole Bay, the

786 estimated primary production far exceeds the average estimated benthic macrofaunal respiration .

787 Kemp et al. (1997) estimated benthic respiration by combining sulfate reduction and sediment

788 oxygen consumption rates, which together account for both microbial and macrofaunal

789 respiration. Their results suggest that benthic respiration is a smaller fraction of NPP in the Mid

790 and Lower Bay, compared to the Upper Bay. This may reflect the relatively modest role of

791 macrofaunal respiration in these lower-biomass regions, despite higher autochthonous production

792 and organic carbon delivery to the sediments. Our estimates of benthic macrofaunal respiration

793 as a fraction of the total input of organic carbon to the mainstem (3–8%) is slightly lower than

794 estimates derived by Hopkinson & Smith (2004) and Rodil et al. (2022). Hopkinson & Smith,

795 (2004) estimated that approximately 24% of total available organic carbon is respired by the

796 benthos, while Rodil et al. (2022) found that benthic macrofauna account for roughly 40% of

797 total benthic respiration. Taken together, these studies suggest that around 10% of the total input

798 of organic carbon is expected to be respired by benthic macrofauna. Although the Bay-wide

799 fraction is small, macrofaunal respiration may still dominate locally in specific hotspots.

800   Unlike the extensive research on estuarine benthic respiration, benthic macrofaunal

801 calcification has received relatively little attention. Yet our findings suggest it may play a

802 significant role in the Chesapeake Bay carbon budget. As shown in Table 3, bivalves sampled

803 through the BMP program contribute substantially to calcification, surpassing calcification by

804   present-day Eastern oyster populations but comparable to that of historic populations in the

805   mainstem Bay. The importance of bivalve calcification is further emphasized when considering

806   calcium dynamics. To place bivalve calcification in context, we assumed that all riverine calcium

807   inputs were available for shell production. This is an upper-bound estimate because oceanic

808   calcium greatly exceeds riverine fluxes (Beckwith et al., 2019). While not a full calcium budget,

809   the comparison highlights how large the demand from calcification could be relative to the much

810   smaller riverine supply. Alkalinity fluxes further highlight the biogeochemical significance of

811   calcification. For the whole Bay, our estimated alkalinity consumption from benthic macrofaunal

812   calcification of 2.52 ± 1.13 mol m^{-2} yr^{-1} (6.90 ± 3.10 mmol m^{-2} day^{-1}) accounts for more than half

813   of the Bay-wide alkalinity sink estimated by Waldbusser et al. (2013) at 12 mmol m^{-2} day^{-1}. In

814   the Potomac River Estuary, our estimated alkalinity sink due to benthic calcification

815   (6.31 ± 2.84 mol m^{-2} yr^{-1} or 17.29 ± 7.78 mmol m^{-2} day^{-1}) is comparable to the alkalinity sink of

816   22 ± 1 mmol m^{-2} day^{-1} estimated by Najjar et al. (2020), who proposed that *C. fluminea* was

817   primarily responsible. Our findings, highlighting contributions from both *R. cuneata* and *C.*

818   *fluminea*, support their hypothesis and emphasize the substantial role of benthic calcification in

819   modulating alkalinity in estuaries.

820   Benthic macrofauna may play a major role in CO_2 outgassing, as indicated by our

821   estimated CO_2 fluxes from benthic macrofauna in the Upper Bay and upper tributaries, which

822   exceed typical CO_2 fluxes at the air–sea interface. Our benthic macrofaunal CO_2 generation

823   estimates for the Upper Bay (151 g C m^{-2} yr^{-1}), where bivalve biomass is concentrated, exceed

824   those reported by Chauvaud et al. (2003), who estimated 55 ± 51 g C m^{-2} yr^{-1} of CO_2 production

825   from calcification and respiration by the bivalve *P. amurensis* in northern San Francisco Bay.

826   Our results support their hypothesis that benthic calcifiers can serve as major CO_2 generators in

827 estuaries. Not all of this CO_2 generated would be outgassed. However, the combination of a TA

828 sink and DIC source from the bivalves leads to elevated pCO_2, enhancing the potential for

829 increased CO_2 outgassing (Middelburg et al., 2020). Given the high heterotrophy in the Upper

830 Bay and upper tributaries, as well as the balance between benthic macrofaunal respiration and

831 the total input of organic carbon to the Potomac River Estuary, it is conceivable that benthic

832 macrofauna are major contributors to CO_2 outgassing in these regions.

833   Although our empirical framework presented here captures the dominant patterns of

834 benthic secondary production, it does not explicitly incorporate seasonal temperature variability.

835 Because we applied summer temperatures associated with biomass, our production estimates

836 likely represent the upper end of expected values. A simple sensitivity analysis comparing

837 summer and winter conditions suggests that production, and by extension calcification and

838 respiration, may be closer to 60% of the values reported here under mean annual cycles.

839 Importantly, this potential bias is encompassed within our uncertainty bounds and therefore does

840 not affect our overall conclusions.

841 **4.2. Environmental controls on benthic biomass distribution**

842   Bivalve species distribution within the Bay is primarily driven by salinity tolerances.

843 Both the GAMs analysis (Table 5) and the biomass densities associated with salinity zones (Fig.

844 3) showed that benthic biomass, dominated by bivalves, was much higher at lower salinities. The

845 strong influence of salinity on benthic fauna distribution within estuaries has long been

846 recognized (Cain, 1975; Hopkins et al., 1973). This relationship is illustrated in our study by the

847 preference of the most abundant species, *R. Cuneata*, *L. balthica*, and *C. fluminea*, for less saline

848 water. *R. Cuneata* is widely known to need less saline waters, optimally between 1 and 15 ppt, to

849 survive (Hopkins et al., 1973). *C. fluminea* prefers freshwater environments (Phelps, 1994; Sousa

850   et al., 2008). *L. balthica* has a range of tolerances but abundance declines below 5 ppt (Jansson et

851   al., 2015). In our study, *L. balthica* is more concentrated between 5 and 13 ppt. While salinity

852   determines which species dominate, other factors influence their relative abundances within

853   salinity zones.

854   Within mesohaline zones, summer hypoxia appears to be driving extremely low benthic

855   biomass. In our GAMs analysis, an association existed between low biomass and extremely low

856   bottom dissolved oxygen values. Among the different salinity zones, low biomass is associated

857   with low dissolved oxygen in the high mesohaline, where we had the lowest biomass densities.

858   Long-term exposure to hypoxia (<2 mg L^{-1} or 62.5 mmol m^{-3}) is often fatal to benthic

859   macrofauna (Diaz et al., 1995; Seitz et al., 2006; Seitz et al., 2009) and many benthic

860   communities (approximately 50%) only recover on an annual timescale (Diaz et al., 1995). In

861   other words, regions that suffer frequent hypoxia often see lower levels of benthic biomass even

862   when hypoxic conditions are not occurring. In the Chesapeake Bay, hypoxia is most likely to

863   occur in the deeper, mesohaline regions (Frankel et al., 2022; Zheng & DiGiacomo, 2020),

864   providing evidence that our suppressed values of benthic macrofauna at this salinity zone could

865   be due to mass mortality from hypoxia. This pattern is particularly evident where biomass is

866   extremely low through the Mid Bay and lower Potomac River Estuary, regions typically

867   associated with summer hypoxia (Sturdivant et al., 2013).

868   Across the Bay, the relatively narrow range of summer bottom water temperatures likely

869   explains why temperature has an insignificant effect on the spatial distribution of benthic

870   biomass. In our GAMs analysis, summer bottom water temperature was not significantly

871   correlated with benthic biomass. Water temperature has been considered an important driver of

872   benthic biomass (Marsh & Tenore, 1990; Seitz et al., 2006; Seitz et al., 2009; Testa et al., 2020),

873 with low temperature specifically creating mass mortality of *R. cuneata* during winter and spring

874 (Tuszer-Kunc et al., 2020). Higher temperature, however, will drive early and larger seasonal

875 hypoxia in the Chesapeake Bay (Hinson et al., 2022; Irby et al., 2018; Ni et al., 2019). So,

876 temperature could still indirectly affect benthic biomass through its effect on dissolved oxygen.

877 Therefore, while temperature many not directly drive spatial patterns of biomass, it could be

878 more relevant to temporal changes in biomass.

879   Although NO_3^- is a strong predictor of benthic biomass, the mechanisms are likely

880 complex and not necessarily linked to autochthonous primary production. In upper estuarine

881 zones, high NO_3^- concentrations are often associated with elevated suspended solid loads, which

882 limit light and may inhibit autotrophy (Brush et al., 2020b). Yet these same areas show strong

883 heterotrophy, suggesting that respiration exceeds local production. Prior studies have shown that

884 POC in upper estuaries contains substantial terrigenous inputs (Canuel & Hardison, 2016), and

885 respiration of this organic matter likely contributes to heterotrophy in these regions (Kemp et al.,

886 1997; Testa et al., 2020). This pattern raises the possibility that NO_3^- may serve as a proxy for

887 allochthonous POC delivery. Supporting this, USGS data compiled by Zhang & Blomquist

888 (2018) indicate that tributaries with high NO_3^- also tend have high loads of POC. However,

889 further study is needed to test this hypothesis, and the observed NO_3^-–POC correlation should

890 not be interpreted as causal.

891   Our model explained roughly half of the deviance in biomass, indicating that

892 environmental predictors captured key bottom-up controls. However, our model did not account

893 for top-down factors such as predation, which may also play a significant role in shaping

894 biomass distributions, particularly in an estuary with a densely populated watershed and

895 substantial fishing pressure.

Conclusion

This study quantifies estuarine-scale benthic macrofaunal biomass and associated carbon fluxes, including secondary production, respiration, and calcification, across the Chesapeake Bay. The results demonstrate that benthic macrofauna play a substantial and spatially structured role in estuarine carbon cycling, particularly in upper estuarine zones where biomass is highest. In these regions, benthic macrofauna respiration is a significant fraction of total available organic carbon inputs, up to 45%, while calcification accounts for a large portion of the observed alkalinity sink. These contributions vary across the salinity gradient, shaped by both environmental drivers and taxonomic composition.

Patterns observed in this study suggest that benthic biomass and its associated carbon fluxes are influenced by gradients in salinity, oxygen, and organic matter inputs. The dominance of bivalves in low-salinity zones has particularly strong biogeochemical implications due to the role of bivalves in secondary production and calcification. Notably, NO_3^- emerged as a strong predictor of benthic biomass, not necessarily due to enhanced autotrophic production, but potentially reflecting allochthonous organic matter inputs that drive heterotrophic metabolism. The significant contributions of benthic communities to alkalinity consumption and DIC release highlight their potential to alter estuarine carbon chemistry in ways that depend on both biological composition and environmental conditions.

To build on these results, future work should examine how benthic biomass and associated carbon fluxes vary over time in response to both natural variability and anthropogenic change. Predicting future responses is especially challenging due to the high-frequency variability in estuarine systems, which can obscure long-term signals. Understanding how POC inputs, particularly allochthonous sources, change seasonally and interannually will be critical, as

919   will clarifying the extent to which NO_3^- serves as a proxy for those inputs. Long-term monitoring

920   and modeling efforts that link changes in watershed nutrient loading, land use, and climate with

921   benthic community dynamics will be essential for forecasting ecosystem responses and for

922   developing more accurate, responsive biogeochemical models. These predictive relationships

923   between benthic biomass and environmental conditions could also support management and

924   restoration planning. By identifying areas where oxygen, salinity, or sediment improvements are

925   most likely to enhance benthic productivity, the models provide a framework for prioritizing

926   restoration efforts and assessing ecosystem responses to changing conditions.

927

928

929

930

931

932

933

934

935

936

937

938

939

940

941

942 **Appendix A**

943 *Biomass Sampling Density*

944   This appendix shows the spatial distribution of sampling effort for the BMP from 1995 to

945 2022. Fig. A1 illustrates the number of samples collected in each grid cell, highlighting areas of

946 higher and lower sampling density across the Chesapeake Bay and its tributaries.

947
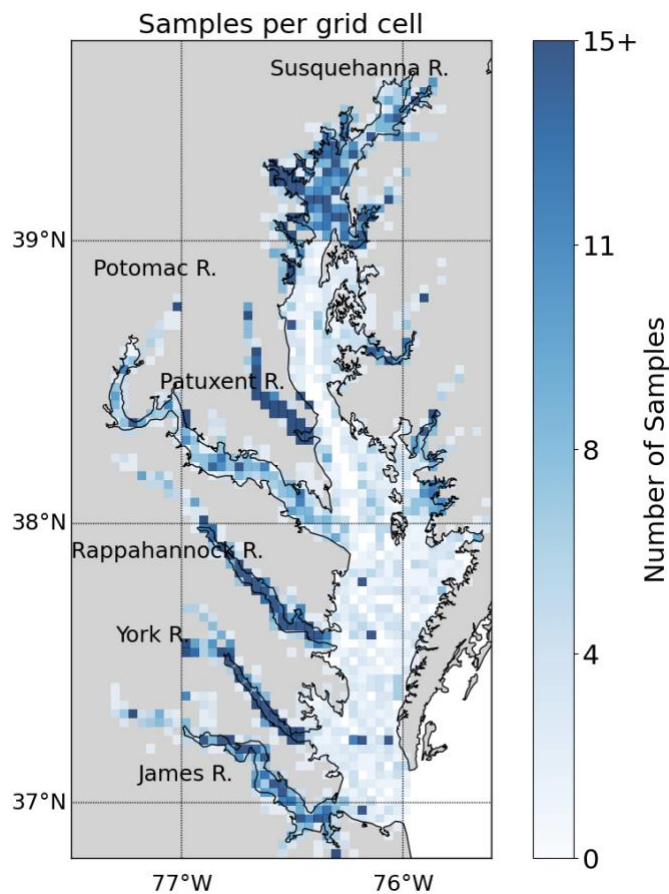
948 Figure A1: Number of benthic samples collected in each grid cell in the summer (July 15 to

949 September 30) from 1995 to 2022 from the Chesapeake Bay Benthic Monitoring Program. The

950 grids are approximately square, measuring 3.5 km by 3.5 km. Each grid cell contains a time-

951 average of each measurement collected in the cell

952 **Appendix B**

953 *Carbon flux uncertainties*

954   This appendix explains the methodology for propagating uncertainty in the benthic

955 macrofaunal carbon flux estimates. It outlines the parameter ranges used, the calculations for

956 uncertainty bounds, and the assumptions underlying these estimates. These details support the

957 uncertainty ranges shown in figures and tables in the Results section. Uncertainty estimates were

958 propagated through empirical equations using standard error propagation techniques (Taylor,

959 2022) assuming uncorrelated inputs and approximating relative errors when only a range of

960 values was available.

961   Uncertainty for carbon-based biomass (B_c) is derived from the two different r_c values:

962
$$\frac{\Delta B_c}{B_c} = \frac{\Delta r_c}{r_c} \tag{B1}$$

963 where $\Delta r_c = 0.03$ g C g^{-1}, half the range of possible r_c values.

964   The uncertainty for the first approach for estimating secondary production (S_1) is derived

965 from B_c and α:

966
$$\frac{\Delta S_1}{S} = \sqrt{\left(\frac{\Delta \alpha}{\alpha}\right)^2 + \left(\frac{\Delta B_c}{B_c}\right)^2} \tag{B2}$$

967 $\Delta \alpha$ is half the range of possible α values and equals 1.695 yr^{-1}.

968   Uncertainty in secondary production (S) arises from the multiple equations used:

969
$$\frac{\Delta S}{S} = \sqrt{w\left(\frac{\Delta S_1}{S_1}\right)^2 + 2w\varepsilon} \tag{B3}$$

970 where each model is equally weighted ($w = 1/3$). Only Model 1 (Equation 5) includes an explicit

971 source of uncertainty, while Models 2 and 3 (Equations 7 and 8) do not. Therefore a small error

972 term $\varepsilon = 0.001$ was assumed for those two models.

973   Calcification (C) uncertainty is derived from r_s and S:

974 $$\frac{\Delta C}{C} = \sqrt{\left(\frac{\Delta r_s}{r_s}\right)^2 + \left(\frac{\Delta S}{S}\right)^2} \tag{B4}$$

975 where r_s has one value for *C. fluminea* and one for *P. amurensis*. $\Delta r_s = 2.5$ g CaCO3 (g C)$^{-1}$ and

976 is half the range of possible r_s values.

977 The uncertainty in respiration (R) is derived solely from S:

978 $$\Delta R = 2.33\Delta S \tag{B5}$$

979 The uncertainties in the fluxes of alkalinity and DIC (F_{TA} and F_{DIC}) are also derived from

980 C and R:

981 $$\Delta F_{TA} = \frac{-2\Delta C}{M_{CaCO_3}} \tag{B6}$$

982 $$\Delta F_{DIC} = \sqrt{\left(\frac{\Delta R}{M_C}\right)^2 + \left(\frac{\Delta C}{M_{CaCO_3}}\right)^2} \tag{B7}$$

983 where M_{CaCO_3} and M_C are the molar masses of CaCO3 and C, respectively.

984 Finally, we propagate the error in the flux of carbon dioxide (F_{CO_2}) from the errors in F_{TA}

985 and F_{DIC}:

986 $$\Delta F_{CO_2} = \sqrt{\left(\frac{[CO_2]\zeta_{TA}\,\Delta F_{TA}}{[TA]}\right)^2 + \left(\frac{[CO_2]\,\zeta_{DIC}\Delta F_{DIC}}{[DIC]}\right)^2} \tag{B8}$$

987 We do not consider errors in the buffer factors, [CO2], [DIC], and [TA] in ROMS.

988 **Appendix C**

989 ***Secondary production model comparison***

990 This appendix details the comparison of secondary production estimates from the three

991 approaches described in Section 2.3.1. Seasonal and spatial variations are shown to illustrate the

992   influence of temperature and other parameters on production estimates. These comparisons

993   provide context for interpreting model differences presented in the main text.

994
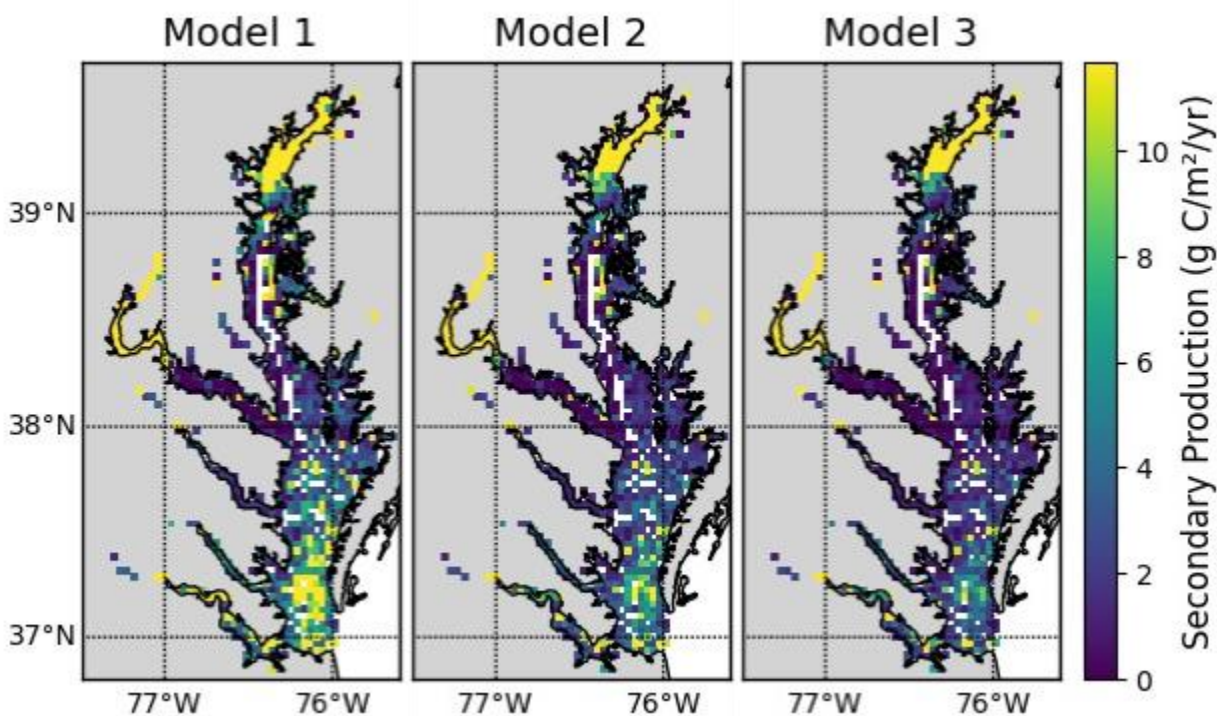
995   Figure C1: Long-term average secondary production across the Chesapeake Bay for each of the

996   three secondary production models.

997   The models have similar spatial patterns (Fig. C1), which are similar to the pattern of

998   benthic biomass (Fig. 2). Secondary production is generally higher in Model 1 than in Models 2

999   and 3, which can be seen most clearly in the means, which are 17.92, 8.31, and 7.59 g C m^{-2} yr^{-1}

1000   in Models 1, 2, and 3, respectively.

1001
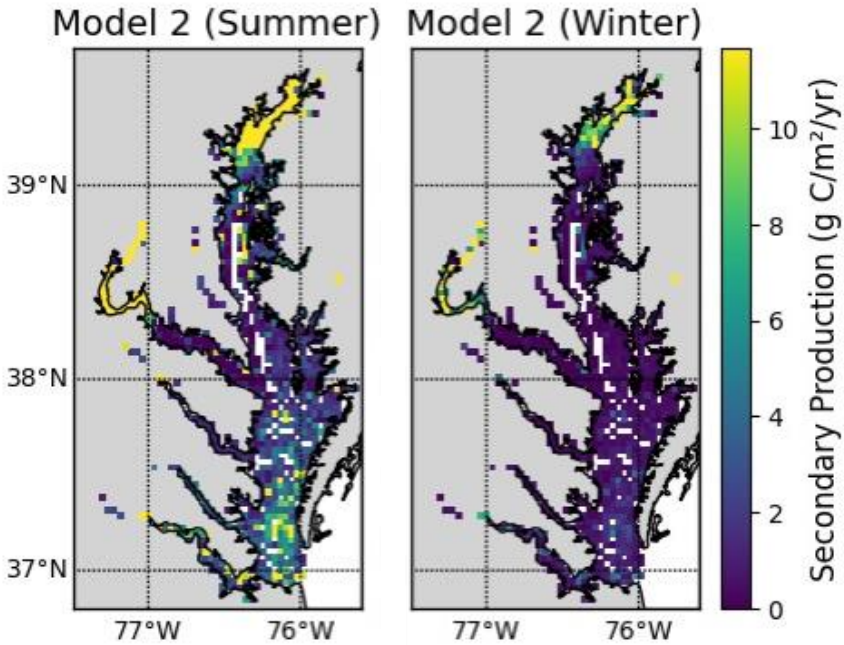
1002 Figure C2: Seasonal sensitivity of Model 2 to bottom temperature inputs.

1003 Fig. C2 and C3 compare secondary production between summer and winter scenarios.

1004 The summer scenario uses summer bottom water temperatures measured concurrently with

1005 biomass samples, while the winter scenario assumes a temperature of 1 °C. Fig. C2 shows the

1006 results for Model 2, which has a mean secondary production of 8.31 g C m^{-2} yr^{-1} in summer and

1007 1.89 g C m^{-2} yr^{-1} in winter. Fig. C3 shows the results for Model 3, which has a mean secondary

1008 production of 7.59 g C m^{-2} yr^{-1} in summer and 1.44 g C m^{-2} yr^{-1} in winter. For both models,

1009 production in summer is about 5 times that of winter, as expected from the rough estimates in the

1010 Methods section. Assuming spring and fall are halfway between winter and summer, and

1011 weighting the seasons equally, the annually averaged secondary production rate would be about

1012 60% of the summer rate.

1013
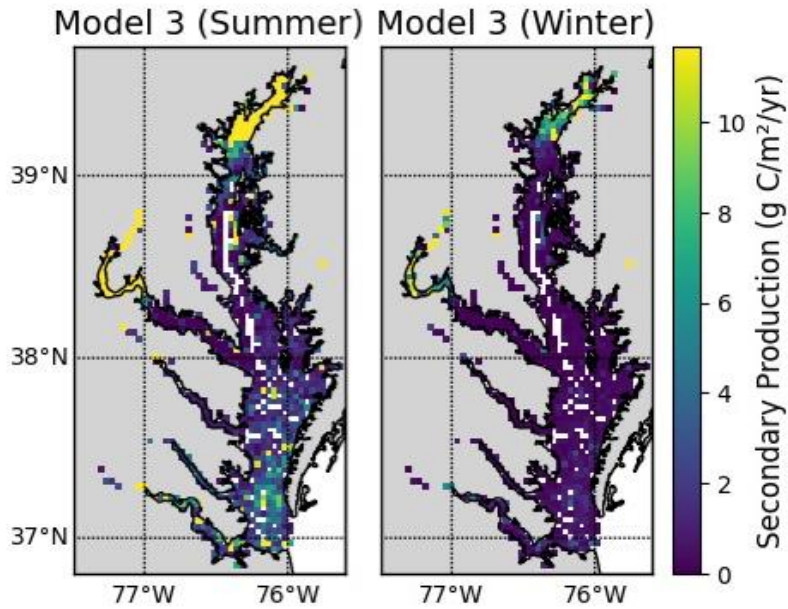
1014   Figure C3: Seasonal sensitivity of Model 3 to bottom temperature inputs.

1015   **Appendix D**

1016   *Species biomass distribution*

1017   This appendix expands on the biomass distribution results in Section 3.1 by showing

1018   detailed spatial patterns for individual species and taxonomic classes. Fig. D1 complements the

1019   summary figures in the main text, highlighting species-specific habitat associations.

1020
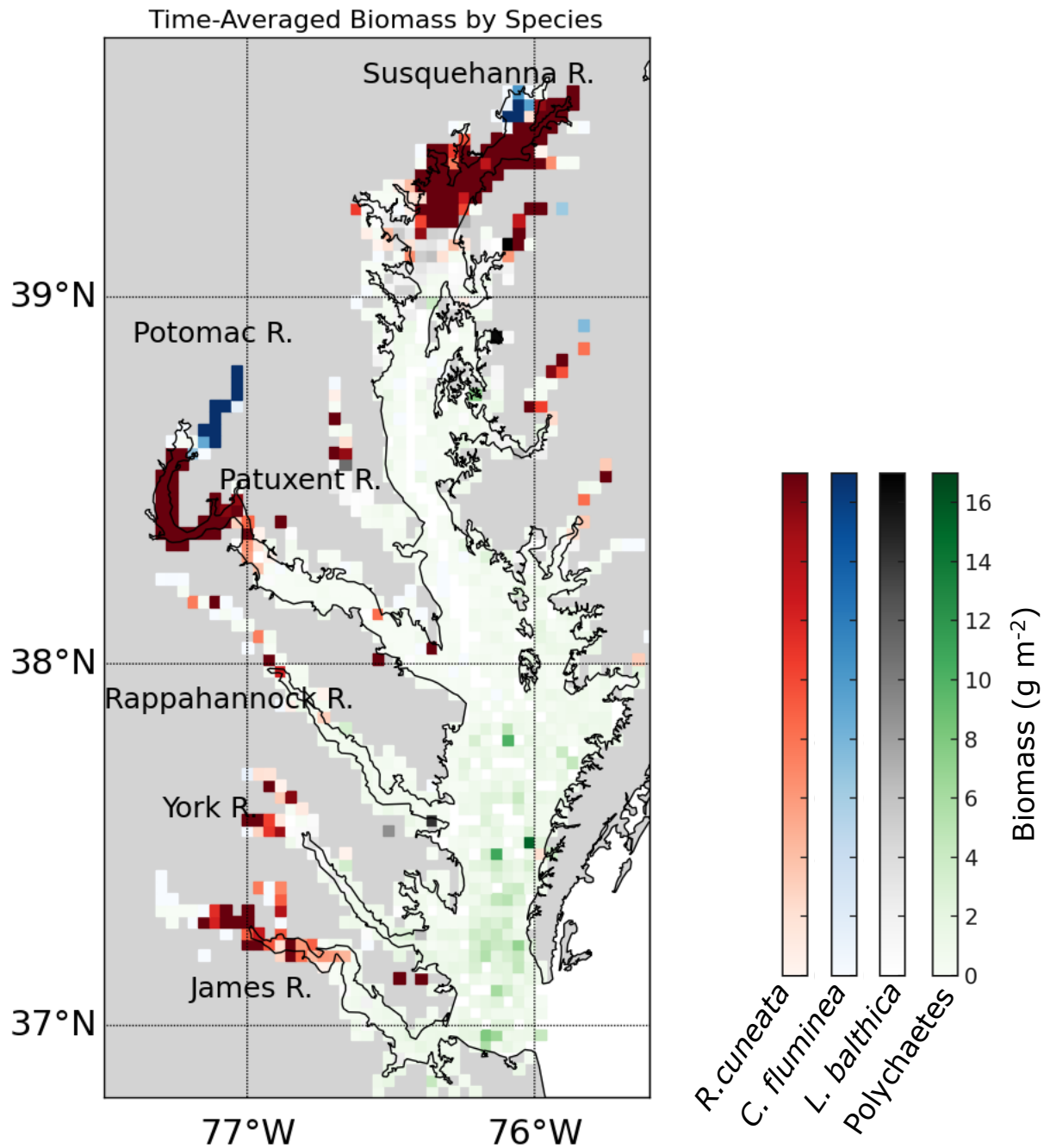
1021 Figure D1: Average summer biomass density from 1995 to 2022 from the Maryland and Virginia

1022 Benthic Monitoring Program. Each color corresponds to a specific bivalve species (*M. balthica,*

1023 *C. fluminea, or R. cuneata*) or polychaetes. The color shown on the map is the species with the

1024 highest time-averaged biomass in that grid cell.

1025 **Appendix E**

1026   *Carbon flux-related parameters*

1027   To illustrate estuarine variability in carbonate system drivers, we summarized a suite of

1028   flux and water column properties across tidal salinity zones of the Chesapeake Bay (Fig. E1).

1029   The patterns highlight strong gradients from tidal fresh through polyhaline regions. Notably

1030   [CO_2] is elevated in tidal fresh waters, underscoring the combined influence of salinity, TA, and

1031   the TA:DIC ratio on estuarine carbonate chemistry.
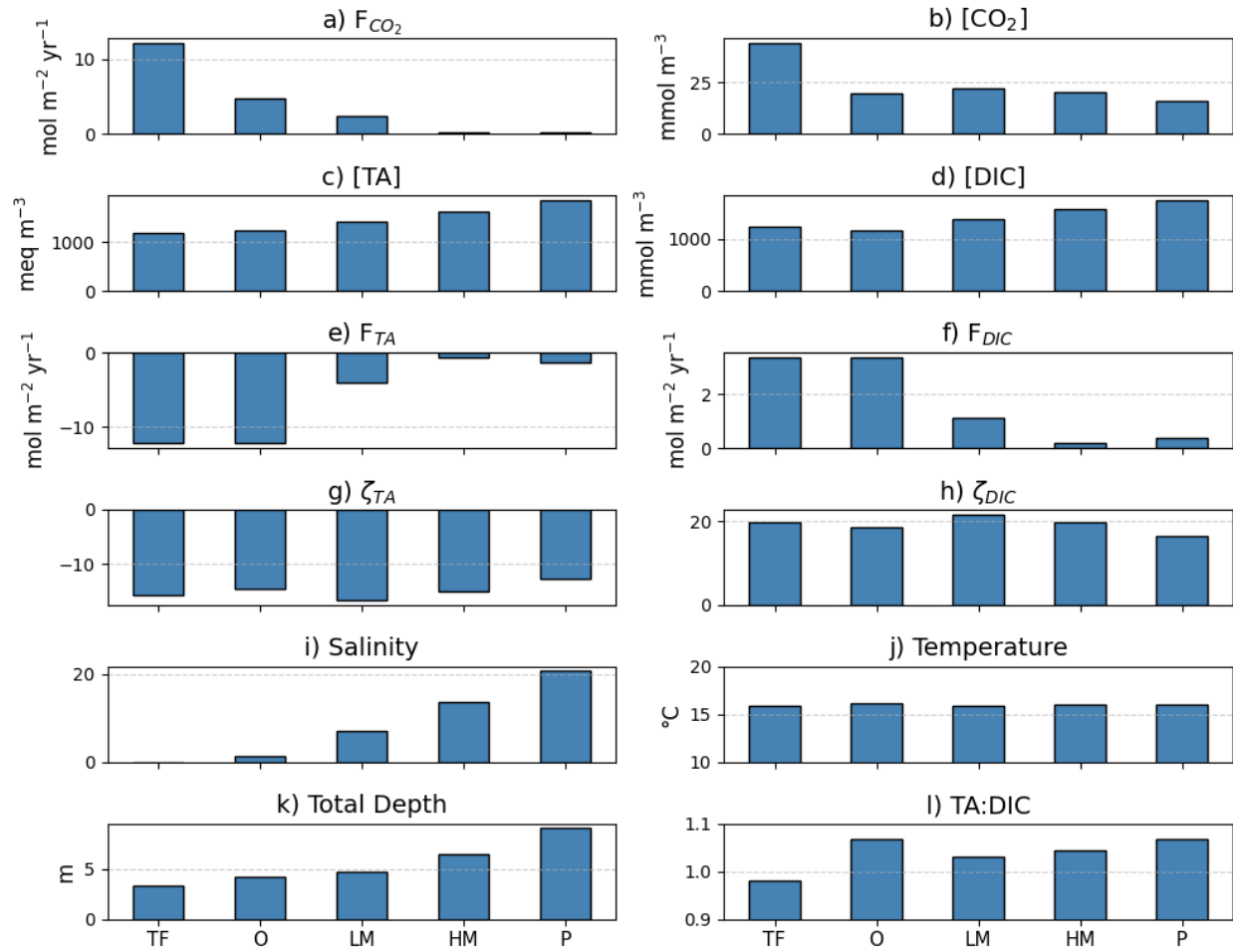
1033   Figure E1: Carbon flux-related parameters averaged within salinity zones of Chesapeake Bay.

1034   [CO_2] was calculated using PyCO2SYS; temperature, salinity, total depth, [TA] and [DIC] were

1035   obtained from ROMS model output. F_{TA} and F_{DIC} were calculated following Equations 12–13,

1036 ζ_{TA} and ζ_{DIC} from Equations 15–16, and F_{CO_2} from Equation 14.

1037 **Appendix F**

1038 *GAMs evaluation*

1039   This appendix presents diagnostic plots and statistics for the generalized additive models

1040 described in Section 2.5. Residual maps, histograms, and fitted-vs-observed plots (Fig. F1) are

1041 included to evaluate model performance and identify patterns in prediction errors.

1042   A good model would have points on a modeled vs. observed scatterplot fall close to a 1:1

1043 line and have the departures from that line (residuals) be close to normally distributed. Although

1044 GAMs can handle non-normal distributions of the response variable (Guisan et al., 2002), we

1045 found the best model fit by applying a natural logarithmic transformation to the biomass. A small

1046 constant (0.0001 g m^{-2}) was added to the biomass values before applying the natural logarithmic

1047 transformation to account for zeros in the data. The resulting biomass was normally distributed

1048 after applying the natural logarithm function, so the GAM was fitted with a Gaussian distribution

1049 with an identity link function.

1050
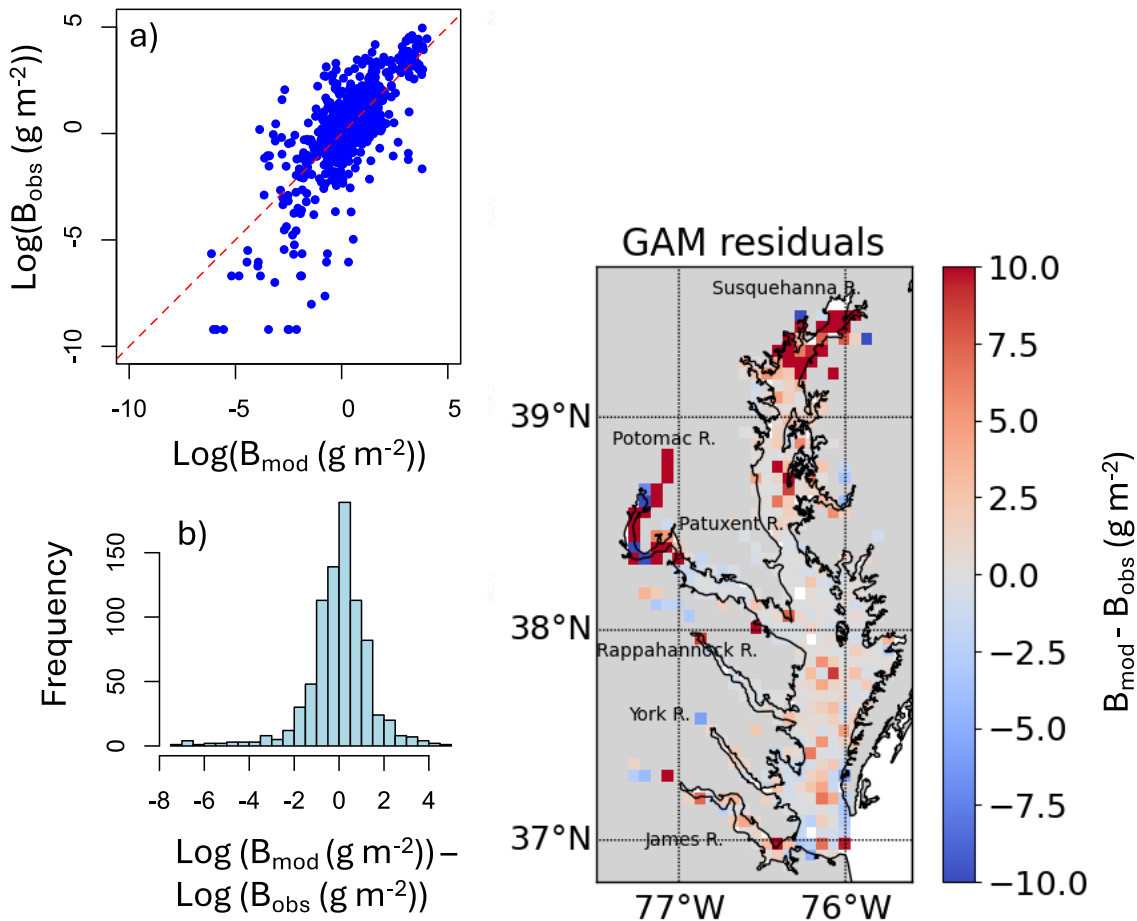
1051
1052   Figure F1: Evaluation of the total biomass GAM, which includes O_2, salinity, total depth, NO_3^-,

1053   sand fraction, and water temperature as predictor variables. "Log" refers to the natural logarithm.

1054   (a) Modeled vs. observed values. (b) Histogram of biomass residuals (modeled minus observed

1055   values, $B_{mod} - B_{obs}$). (c) Spatial distribution of the residuals.

1056

1057   **Data Availability**

1058   All data used in this study are publicly available and have been described in the Methods section.

1059   Water quality data were obtained from the *Chesapeake Bay Water Quality Monitoring Program*

1060   (https://datahub.chesapeakebay.net/WaterQuality), and benthic data were sourced from the

1061   *Chesapeake Bay Long-Term Benthic Monitoring Program*

1062   (https://www.baybenthos.versar.com/data.htm). Model output used in this study is publicly

1063   available at https://www.seanoe.org/data/00882/99441/.

1064

1065   **Author Contribution**

1066   SA led the research, conducted data analysis, interpreted results, and wrote the initial and

1067   subsequent drafts of the manuscript.

1068   RN conceptualized the project, defined overarching research goals, secured financial support,

1069   and contributed substantially to manuscript drafts through critical reviews, commentary, and

1070   revisions.

1071   ER provided significant insights from her expertise on the physiological responses of marine

1072   invertebrates to environmental variables, influencing the scope and direction of the study. She

1073   also substantially contributed to manuscript revisions through critical reviews and commentary.

1074   RW contributed significant expertise on benthic biomass distribution in Chesapeake Bay and

1075   generalized additive modeling techniques, shaping the analytical framework of the study. He

1076   provided critical feedback and revisions during manuscript preparation.

1077   MF provided ongoing feedback throughout the research process, particularly regarding the

1078   integration of modeling information and interpretation of results, and contributed critical

1079   commentary on multiple presentations of the work.

1080   PS consistently provided feedback and contributed modeling expertise, assisting with data

1081   interpretation and manuscript revisions through critical reviews and commentary.

1082   SD developed the original empirical models linking benthic macrofaunal biomass to carbon

1083   fluxes, laying foundational methodological contributions to the study.

1084

Competing Interests

The authors declare that they have no conflict of interest.

Acknowledgements

We thank Maria Herrmann, Jill Arriola, and Alexa Labossiere for their valuable discussions and

feedback that contributed to this manuscript. We also acknowledge Riley Westman and Edward

Stets for providing riverine calcium input data from the USGS. Additionally, we used AI tools,

including Grammarly and ChatGPT, to assist with grammar and clarity in sentence editing.

Financial Support

This work is supported by the National Science Foundation (NSF) Chemical and Biological

Oceanography Program under Grant Nos. OCE-2148949 (Penn State), OCE-2148950 (VIMS),

and OCE-2148952 (UMCES), and by the U.S. Department of Energy's Biological and

Environmental Research Program as part of the Integrated Coastal Modeling project.

References

1108 **References**

1109 Akoglu, H. (2018). User's guide to correlation coefficients. *Turkish Journal of Emergency*
1110   *Medicine*, *18*(3), 91–93. https://doi.org/10.1016/j.tjem.2018.08.001
1111 Beckwith, S. T., Byrne, R. H., & Hallock, P. (2019). Riverine calcium end-members improve
1112   coastal saturation state calculations and reveal regionally variable calcification potential.
1113   *Frontiers in Marine Science*, *6*(APR). https://doi.org/10.3389/fmars.2019.00169
1114 Birchenough, S. N. R., Reiss, H., Degraer, S., Mieszkowska, N., Borja, Á., Buhl-Mortensen, L.,
1115   Braeckman, U., Craeymeersch, J., De Mesel, I., Kerckhof, F., Kröncke, I., Parra, S., Rabaut,
1116   M., Schröder, A., Van Colen, C., Van Hoey, G., Vincx, M., & Wätjen, K. (2015). Climate
1117   change and marine benthos: A review of existing research and future directions in the North
1118   Atlantic. *Wiley Interdisciplinary Reviews: Climate Change*, *6*(2), 203–223.
1119   https://doi.org/10.1002/wcc.330
1120 Borja, A., Dauer, D. M., Díaz, R., Llansó, R. J., Muxika, I., Rodríguez, J. G., & Schaffner, L.
1121   (2008). Assessing estuarine benthic quality conditions in Chesapeake Bay: A comparison of
1122   three indices. *Ecological Indicators*, *8*(4), 395–403.
1123   https://doi.org/10.1016/j.ecolind.2007.05.003
1124 Brey, T. (1990). Confidence limits for secondary production estimates: Application of the
1125   bootstrap to the increment summation method. *Marine Biology*, *106*, 503–508.
1126 Brush, M. J., Mozetič, P., Francé, J., Aubry, F. B., Djakovac, T., Faganeli, J., Harris, L. A., &
1127   Niesen, M. (2020). Phytoplankton dynamics in a changing environment. In T. C. Malone,
1128   A. Malej, & J. Faganeli (Eds.), *Coastal Ecosystems in Transition: A Comparative Analysis*
1129   *of the Northern Adriatic and Chesapeake Bay* (pp. 49–74). Wiley.
1130   https://doi.org/10.1002/9781119543626.ch4
1131 Cain, T. D. (1975). Reproduction and recruitment of the brackish water clam, Rangia cuneata in
1132   the James River, Virginia. *Fishery Bulletin*, *73*(2), 412.
1133   https://scholarworks.wm.edu/vimsarticles/2139
1134 Canuel, E. A., & Hardison, A. K. (2016). Sources, ages, and alteration of organic matter in
1135   estuaries. *Annual Review of Marine Science*, *8*, 409–434. https://doi.org/10.1146/annurev-
1136   marine-122414-034058
1137 Cerco, C. F., & Noel, M. R. (2010). Monitoring, modeling, and management impacts of bivalve
1138   filter feeders in the oligohaline and tidal fresh regions of the Chesapeake Bay system.
1139   *Ecological Modelling*, *221*(7), 1054–1064. https://doi.org/10.1016/j.ecolmodel.2009.07.024
1140 Chauvaud, L., Thompson, J. K., Cloern, J. E., & Thouzeau, G. (2003). Clams as CO2 generators:
1141   The Potamocorbula amurensis example in San Francisco Bay. *Limnology and*
1142   *Oceanography*, *48*(6), 2086–2092. https://doi.org/10.4319/lo.2003.48.6.2086
1143 Chen, C. T. A., Huang, T. H., Chen, Y. C., Bai, Y., He, X., & Kang, Y. (2013). Air–sea
1144   exchanges of CO2 in the world's coastal seas. *Biogeosciences*, *10*(10), 6509–6544.
1145   https://doi.org/10.5194/bg-10-6509-2013
1146 Chesapeake Bay Program. (n.d.). *CBP Water Quality Database (1984-present)*.
1147 *Chesapeake Bay Program analytical segmentation scheme: Revisions, decisions and rationales,*
1148   *1983–2003*. (2004).
1149 Dauer, D. M. (1993). Biological criteria, environmental health and estuarine macrobenthic
1150   community structure. *Marine Pollution Bulletin*, *26*(5), 249–257.
1151   https://doi.org//10.1016/0025-326X(93)90063-P

Dauer, D. M., & Alden III, R. W. (1995). Long-term trends in the macrobenthos and water quality of the lower Chesapeake Bay (1985-1991). *Marine Pollution Bulletin*, *30*(12), 840–850.

Dauer, D. M., & Lane, M. F. (2010). *Quality Assurance/Quality Control Plan: Benthic Biological Monitoring Program of the Lower Chesapeake Bay (July 1, 2010 to June 30, 2011)*.

Dauer, D. M., Ranasinghe, J. A., & Weisberg, S. B. (2000). Relationships between benthic community condition, water quality, sediment quality, nutrient loads, and land use patterns in Chesapeake Bay. *Estuaries*, *23*(1), 80–96.

Diaz, R. J., & Rosenberg, R. (2008). Spreading dead zones and consequences for marine ecosystems. *Science*, 926–929. https://www.science.org

Diaz, R. J., & Schaffner, L. C. (1990). The functional role of estuarine benthos. In M. Haire & E. C. Krome (Eds.), *Perspectives on the Chesapeake Bay* (pp. 25–56). Chesapeake Research Consortium.

Diaz, R., & Rosenberg, R. (1995). Marine benthic hypoxia: A review of its ecological effects and the behavioural responses of benthic macrofauna. *Oceanography and Marine Biology. An Annual Review*, *33*, 245–303. https://www.researchgate.net/publication/236628341

Dolbeth, M., Cusson, M., Sousa, R., & Pardal, M. A. (2012). Secondary production as a tool for better understanding of aquatic ecosystems. *Canadian Journal of Fisheries and Aquatic Sciences*, *69*(7), 1230–1253. https://doi.org/10.1139/F2012-050

Dormann, C. F., Elith, J., Bacher, S., Buchmann, C., Carl, G., Carré, G., García Marquéz, J. R., Gruber, B., Lafourcade, B., Leitão, P. J., Münkemüller, T., McClean, C., Osborne, P. E., Reineking, B., Schröder, B., Skidmore, A. K., Zurell, D., & Lautenbach, S. (2013). Collinearity: A review of methods to deal with it and a simulation study evaluating their performance. *Ecography*, *36*(1), 27–46.

Drexler, M., & Ainsworth, C. H. (2013). Generalized additive models used to predict species abundance in the Gulf of Mexico: An ecosystem modeling tool. *PLoS ONE*, *8*(5). https://doi.org/10.1371/journal.pone.0064458

Edgar, G. J. (1990). The use of the size structure of benthic macrofaunal communities to estimate faunal biomass and secondary production. *Journal of Experimental Marine Biology and Ecology*, *137*(3), 195–214.

Egleston, E. S., Sabine, C. L., & Morel, F. M. M. (2010). Revelle revisited: Buffer factors that quantify the response of ocean chemistry to changes in DIC and alkalinity. *Global Biogeochemical Cycles*, *24*(1). https://doi.org/10.1029/2008GB003407

Ehrnsten, E., Norkko, A., Timmermann, K., & Gustafsson, B. G. (2019). Benthic-pelagic coupling in coastal seas – Modelling macrofaunal biomass and carbon processing in response to organic matter supply. *Journal of Marine Systems*, *196*, 36–47. https://doi.org/10.1016/j.jmarsys.2019.04.003

Eleftheriou, A., & Moore, D. C. (2013). Macofauna techniques. *Methods for the Study of Marine Benthos*, 175–251.

Frankel, L. T., Friedrichs, M. A. M., St-Laurent, P., Bever, A. J., Lipcius, R. N., Bhatt, G., & Shenk, G. W. (2022). Nitrogen reductions have decreased hypoxia in the Chesapeake Bay: Evidence from empirical and numerical modeling. *Science of the Total Environment*, *814*. https://doi.org/10.1016/j.scitotenv.2021.152722

Frankignoulle, M., Abril, G., Borges, A., Bourge, I., Canon, C., Delille, B., Libert, E., & Théate, J.-M. (1998). Carbon dioxide emission from European estuaries. *Science*, *282*(5388), 434–436. https://www.science.org

Fulford, R. S., Breitburg, D. L., Newell, R. I. E., Kemp, W. M., & Luckenbach, M. (2007). Effects of oyster population restoration strategies on phytoplankton biomass in Chesapeake Bay: a flexible modeling approach. *Marine Ecology Progress Series*, *336*, 43–1.

Galimany, E., Lunt, J., Freeman, C. J., Houk, J., Sauvage, T., Santos, L., Lunt, J., Kolmakova, M., Mossop, M., Domingos, A., Phlips, E. J., & Paul, V. J. (2020). Bivalve feeding responses to microalgal bloom species in the Indian River Lagoon: the potential for top-down control. *Estuaries and Coasts*, *43*(6), 1519–1532. https://doi.org/10.1007/s12237-020-00746-9

Garcia, H. E., & Gordon, L. I. (1992). Oxygen solubility in seawater: Better fitting equations. *Limnology and Oceanography*, *37*(6), 1307–1312. https://doi.org/10.4319/lo.1992.37.6.1307

Glud, R. N. (2008). Oxygen dynamics of marine sediments. *Marine Biology Research*, *4*(4), 243–289. https://doi.org/10.1080/17451000801888726

Grant, J., & Thorpe, B. (1991). Effects of suspended sediment on growth, respiration, and excretion of the soft-shell clam (Mya arenaria). *Canadian Journal of Fisheries and Aquatic Sciences*, *48*(7).

Grebmeier, J. M., Bluhm, B. A., Cooper, L. W., Denisenko, S. G., Iken, K., Kędra, M., & Serratos, C. (2015). Time-series benthic community composition and biomass and associated environmental characteristics in the Chukchi Sea during the RUSALCA 2004-2012 Program. *Oceanography*, *28*(3), 116–133. https://doi.org/10.2307/24861905

Green, M. A., Waldbusser, G. G., Reilly, S. L., Emerson, K., & O'Donnell, S. (2009). Death by dissolution: Sediment saturation state as a mortality factor for juvenile bivalves. *Limnology and Oceanography*, *54*(4), 1037–1047. https://doi.org/10.4319/lo.2009.54.4.1037

Grüss, A., Drexler, M., & Ainsworth, C. H. (2014). Using delta generalized additive models to produce distribution maps for spatially explicit ecosystem models. *Fisheries Research*, *159*, 11–24. https://doi.org/10.1016/j.fishres.2014.05.005

Guisan, A., Edwards, T. C., & Hastie, T. (2002). Generalized linear and generalized additive models in studies of species distributions: setting the scene. *Ecological Modelling*, *157*(2–3), 89. www.elsevier.com/locate/ecolmodel

Hagy, J. D. (2002). *Eutrophication, hypoxia and trophic transfer efficiency in Chesapeake Bay* [Doctoral dissertation, University of Maryland, College Park]. https://www.researchgate.net/publication/237005296

Harding, L. W., Mallonee, M. E., & Perry, E. S. (2002). Toward a predictive understanding of primary productivity in a temperate, partially stratified estuary. *Estuarine, Coastal and Shelf Science*, *55*(3), 437–463. https://doi.org/10.1006/ecss.2001.0917

Hartwell, S. I., Wright, D. A., Takacs, R., & Hocutt, C. H. (1991). Relative respiration and feeding rates of oyster and brackish water clam in variously contaminated waters. *Marine Pollution Bulletin*, *22*(4), 191–197.

Hastie, T., & Tibshirani, R. (1987). Generalized additive models: Some applications. *Journal of the American Statistical Association*, *82*(398).

Hauke, J., & Kossowski, T. (2011). Comparison of values of Pearson's and Spearman's correlation coefficients on the same sets of data. *Quaestiones Geographicae*, *30*(2), 87–93. https://doi.org/10.2478/v10117-011-0021-1

Herrmann, M., Najjar, R. G., Da, F., Friedman, J. R., Friedrichs, M. A. M., Goldberger, S., Menendez, A., Shadwick, E. H., Stets, E. G., & St-Laurent, P. (2020). Challenges in quantifying air-water carbon dioxide flux using estuarine water quality data: Case study for Chesapeake Bay. *Journal of Geophysical Research: Oceans*, *125*(7). https://doi.org/10.1029/2019JC015610

Herrmann, M., Najjar, R. G., Kemp, W. M., Alexander, R. B., Boyer, E. W., Cai, W. J., Griffith, P. C., Kroeger, K. D., McCallister, S. L., & Smith, R. A. (2015). Net ecosystem production and organic carbon balance of U.S. East Coast estuaries: A synthesis approach. *Global Biogeochemical Cycles*, *29*(1), 96–111. https://doi.org/10.1002/2013GB004736

Hinson, K. E., Friedrichs, M. A. M., St-Laurent, P., Da, F., & Najjar, R. G. (2022). Extent and causes of Chesapeake Bay warming. *Journal of the American Water Resources Association*, *58*(6), 805–825. https://doi.org/10.1111/1752-1688.12916

Hirsch, R. M., Moyer, D. L., & Archfield, S. A. (2010). Weighted regressions on time, discharge, and season (WRTDS), with an application to Chesapeake Bay river inputs. *Journal of the American Water Resources Association*, *46*(5), 857–880. https://doi.org/10.1111/j.1752-1688.2010.00482.x

Holland, A. F., Shaughnessy, A. T., & Hiegel, M. H. (1987). Long-term variation in mesohaline Chesapeake Bay macrobenthos: Spatial and temporal patterns. *Estuaries*, *10*(3), 227–245.

Hopkins, S. H., Anderson, J. W., & Horvath, K. (1973). *The brackish water clam Rangia cuneata as an indicator of ecological effects of salinity changes in coastal waters*.

Hopkinson, C. S., & Smith, E. M. (2004). Estuarine respiration: An overview of benthic, pelagic, and whole system respiration. *Respiration in Aquatic Ecosystems*, 122–146.

Humphreys, M. P., Lewis, E. R., Sharp, J. D., & Pierrot, D. (2022). PyCO2SYS v1.8: Marine carbonate system calculations in Python. *Geoscientific Model Development*, *15*(1), 15–43. https://doi.org/10.5194/gmd-15-15-2022

Irby, I. D., Friedrichs, M. A. M., Da, F., & Hinson, K. E. (2018). The competing impacts of climate change and nutrient reductions on dissolved oxygen in Chesapeake Bay. *Biogeosciences*, *15*(9), 2649–2668. https://doi.org/10.5194/bg-15-2649-2018

Jakubowska, M., & Normant-Saremba, M. (2015). The effect of CO2-induced seawater acidification on the behaviour and metabolic rate of the Baltic clam Macoma balthica. *Annales Zoologici Fennici*, *52*(5–6), 353–367. https://doi.org/10.5735/086.052.0509

Jansson, A., Norkko, J., Dupont, S., & Norkko, A. (2015). Growth and survival in a changing environment: Combined effects of moderate hypoxia and low pH on juvenile bivalve Macoma balthica. *Journal of Sea Research*, *102*, 41–47. https://doi.org/10.1016/j.seares.2015.04.006

Jansson, A., Norkko, J., & Norkko, A. (2013). Effects of reduced pH on Macoma balthica larvae from a system with naturally fluctuating pH-dynamics. *PLoS One*, *8*(6). https://doi.org/10.1371/journal.pone.0068198

Kemp, W. M., Boynton, W. R., Adolf, J. E., Boesch, D. F., Boicourt, W. C., Brush, G., Cornwell, J. C., Fisher, T. R., Glibert, P. M., Hagy, J. D., Harding, L. W., Houde, E. D., Kimmel, D. G., Miller, W. D., Newell, R. I. E., Roman, M. R., Smith, E. M., & Stevenson, J. C. (2005). Eutrophication of Chesapeake Bay: Historical trends and ecological interactions. *Marine Ecology Progress Series*, *303*, 1–29. www.int-res.com

Kemp, W. M., Smith, E. M., Marvin-DiPasquale, M., & Boynton, W. R. (1997). Organic carbon balance and net ecosystem metabolism in Chesapeake Bay. *Marine Ecology Progress Series*, *150*, 229–248.

1288 Kroeker, K. J., Kordas, R. L., Crim, R., Hendriks, I. E., Ramajo, L., Singh, G. S., Duarte, C. M.,
1289   & Gattuso, J. P. (2013). Impacts of ocean acidification on marine organisms: quantifying
1290   sensitivities and interaction with warming. *Global Change Biology*, *19*(6), 1884–1896.
1291   https://doi.org/10.1111/gcb.12179
1292 Levin, L. A., Ekau, W., Gooday, A. J., Jorissen, F., Middelburg, J. J., Naqvi, S. W. A., Neira, C.,
1293   Rabalais, N. N., & Zhang, J. (2009). Effects of natural and human-induced hypoxia on
1294   coastal benthos. In *Biogeosciences* (Vol. 6). www.biogeosciences.net/6/2063/2009/
1295 Little, S., Wood, P. J., & Elliott, M. (2017). Quantifying salinity-induced changes on estuarine
1296   benthic fauna: The potential implications of climate change. *Estuarine, Coastal and Shelf*
1297   *Science*, *198*, 610–625. https://doi.org/10.1016/j.ecss.2016.07.020
1298 Llansó, R. J. (2002). *Methods for calculating the Chesapeake Bay benthic index of biotic*
1299   *integrity*. http://www.baybenthos.versar.com
1300 Llansó, R. J., & Scott, L. (2011). *Chesapeake Bay water quality monitoring program: Long-term*
1301   *benthic monitoring and assessment component, quality assurance project plan, 2011–2012*.
1302 Llansó, R. J., & Zaveta, D. (2017). *Chesapeake Bay water quality monitoring program: Long-*
1303   *term benthic monitoring and assessment component level 1 comprehensive report, July*
1304   *1984 – December 2016 (Volume 1)*.
1305 Marsh, A. G., & Tenore, K. R. (1990). The role of nutrition in regulating the population
1306   dynamics of opportunistic, surface deposit feeders in a mesohaline community. *Limnology*
1307   *and Oceanography*, *35*(3), 710–724. https://doi.org/10.4319/lo.1990.35.3.0710
1308 Meysman, F. J. R., tax, J. J., & Heip, C. H. R. (2006). Bioturbation: A fresh look at Darwin's last
1309   idea. *Trends in Ecology and Evolution*, *21*(12), 688–695.
1310   https://doi.org/10.1016/j.tree.2006.08.002
1311 Middelburg, J. J. (2018). Reviews and syntheses: To the bottom of carbon processing at the
1312   seafloor. In *Biogeosciences* (Vol. 15, Issue 2, pp. 413–427). Copernicus GmbH.
1313   https://doi.org/10.5194/bg-15-413-2018
1314 Middelburg, J. J., Soetaert, K., & Hagens, M. (2020). Ocean alkalinity, buffering and
1315   biogeochemical processes. *Reviews of Geophysics*, *58*(3).
1316   https://doi.org/10.1029/2019RG000681
1317 Mo, C., & Neilson, B. (1994). Standardization of oyster soft tissue dry weight measurements.
1318   *Water Research*, *28*(1), 243–246.
1319 Murphy, R. R., Kemp, W. M., & Ball, W. P. (2011). Long-term trends in Chesapeake Bay
1320   seasonal hypoxia, stratification, and nutrient loading. *Estuaries and Coasts*, *34*(6), 1293–
1321   1309. https://doi.org/10.1007/s12237-011-9413-7
1322 Murphy, R. R., Perlman, E., Ball, W. P., & Curriero, F. C. (2015). Water-distance-based kriging
1323   in Chesapeake Bay. *Journal of Hydrologic Engineering*, *20*(9).
1324   https://doi.org/10.1061/(asce)he.1943-5584.0001135
1325 Najjar, R. G., Herrmann, M., Alexander, R., Boyer, E. W., Burdige, D. J., Butman, D., Cai, W.
1326   J., Canuel, E. A., Chen, R. F., Friedrichs, M. A. M., Feagin, R. A., Griffith, P. C., Hinson,
1327   A. L., Holmquist, J. R., Hu, X., Kemp, W. M., Kroeger, K. D., Mannino, A., McCallister, S.
1328   L., … Zimmerman, R. C. (2018). Carbon budget of tidal wetlands, estuaries, and shelf
1329   waters of Eastern North America. *Global Biogeochemical Cycles*, *32*(3), 389–416.
1330   https://doi.org/10.1002/2017GB005790
1331 Najjar, R. G., Herrmann, M., Cintrón Del Valle, S. M., Friedman, J. R., Friedrichs, M. A. M.,
1332   Harris, L. A., Shadwick, E. H., Stets, E. G., & Woodland, R. J. (2020). Alkalinity in tidal

tributaries of the Chesapeake Bay. *Journal of Geophysical Research: Oceans*, *125*(1). https://doi.org/10.1029/2019JC015597

Nakamura, Y., & Kerciku, F. (2000). Effects of filter-feeding bivalves on the distribution of water quality and nutrient cycling in a eutrophic coastal lagoon. *Journal of Marine Systems*, *26*, 209–221. www.elsevier.nlrlocaterjmarsys

Newell, R. I. E. (1988). Ecological changes in Chesapeake Bay: are they the result of overharvesting the American oyster, Crassostrea virginica. *Understanding the Estuary: Advances in Chesapeake Bay Reserach*, *129*, 536–546.

Newell, R. I. E., & Ott, J. A. (2011). Macrobenthic communities and eutrophication. *Ecosystems at the Land-Sea Margin: Drainage Basin to Coastal Sea*, *55*, 265–293. https://doi.org/10.1029/ce055p0265

Ni, W., Li, M., Ross, A. C., & Najjar, R. G. (2019). Large projected decline in dissolved oxygen in a eutrophic estuary due to climate change. *Journal of Geophysical Research: Oceans*, *124*(11), 8271–8289. https://doi.org/10.1029/2019JC015274

Olson, M. (2012). *Guide to using Chesapeake Bay Program water quality monitoring data*.

Pearson, T. H., & Rosenberg, R. (1978). Macrobenthic succession in relation to organic enrichment and pollution of the marine environment. *Oceanography and Marine Biology: An Annual Review*, *16*, 229–311.

Phelps H.L. (1994). The Asiatic clam (Corbicula fluminea) invasion and system-level ecological change in the Potomac River estuary near Washington, DC. *Estuaries*, *17*(3), 614–621.

Redfield, A. C. (1963). The influence of organisms on the composition of seawater. *The Sea*, 26–77.

Rodil, I. F., Lohrer, A. M., Attard, K. M., Thrush, S. F., & Norkko, A. (2022). Positive contribution of macrofaunal biodiversity to secondary production and seagrass carbon metabolism. *Ecology*, *103*(4). https://doi.org/10.1002/ecy.3648

Rosenberg, R. (1995). Benthic marine fauna structured by hydrodynamic processes and food availibility. *Netherlands Journal of Sea Research*, *34*(4), 303–317.

Rousi, H., Korpinen, S., & Bonsdorff, E. (2019). Brackish-water benthic fauna under fluctuating environmental conditions: the role of eutrophication, hypoxia, and global change. *Frontiers in Marine Science*, *6*(JUL), 464. https://doi.org/10.3389/fmars.2019.00464

Schratzberger, M., & Ingels, J. (2018). Meiofauna matters: the roles of meiofauna in benthic ecosystems. *Journal of Experimental Marine Biology and Ecology*, *502*, 12–25. https://doi.org/10.1016/j.jembe.2017.01.007

Schwinghamer, P., Hargrave, B., Peer, D., & Hawkins, C. M. (1986). Partitioning of production and respiration among size groups of organisms in an intertidal benthic community. *Marine Ecology Progress Series*, *31*(2), 131–142.

Seitz, R. D., Dauer, D. M., Llansó, R. J., & Long, W. C. (2009). Broad-scale effects of hypoxia on benthic community structure in Chesapeake Bay, USA. *Journal of Experimental Marine Biology and Ecology*, *381*(SUPPL.). https://doi.org/10.1016/j.jembe.2009.07.004

Seitz, R., Lipcius, R. N., Olmstead, N. H., Seebo, M. S., & Lambert, D. M. (2006). Influence of shallow-water habitats and shoreline development on abundance, biomass, and diversity of benthic prey and predators in Chesapeake Bay. *Marine Ecology Progress Series*, *326*, 11–27.

Shchepetkin, A. F., & McWilliams, J. C. (2005). The regional oceanic modeling system (ROMS): A split-explicit, free-surface, topography-following-coordinate oceanic model. *Ocean Modelling*, *9*(4), 347–404. https://doi.org/10.1016/j.ocemod.2004.08.002

1379   Simon N. Wood. (2017). *Generalized Additive Models* (2nd ed.).

1380   Smith, M., Paperno, R., Flaherty-Walia, K., & Markwith, S. (2023). Species Distributions in a
1381   Changing Estuary: Predictions Under Future Climate Change, Sea-Level Rise, and
1382   Watershed Restoration. *Estuaries and Coasts*, *46*(6). https://doi.org/10.1007/s12237-023-
1383   01219-5

1384   Snelgrove, P. V. R. (1997). The importance of marine sediment biodiversity in ecosystem
1385   processes. *Ambio*, *26*(8), 578–583. https://doi.org/https://www.jstor.org/stable/4314672

1386   Snelgrove, P. V. R. (1999). Snelgrove, P. V. (1999). Getting to the bottom of marine
1387   biodiversity: sedimentary habitats: ocean bottoms are the most widespread habitat on earth
1388   and support high biodiversity and key ecosystem services. *BioScience*, *42*(2), 129–138.
1389   www.jstor.org

1390   Snelgrove, P. V. R., Soetaert, K., Solan, M., Thrush, S., Wei, C. L., Danovaro, R., Fulweiler, R.
1391   W., Kitazato, H., Ingole, B., Norkko, A., Parkes, R. J., & Volkenborn, N. (2018). Global
1392   carbon cycling on a heterogeneous seafloor. *Trends in Ecology & Evolution*, *33*(2), 96–105.
1393   https://doi.org/10.1016/j.tree.2017.11.004

1394   Sousa, R., Antunes, C., & Guilhermino, L. (2008). Ecology of the invasive Asian clam Corbicula
1395   fluminea (Müller, 1774) in aquatic ecosystems: An overview. In *Annales de Limnologie-*
1396   *International Journal of Limnology* (Vol. 44, Issue 2, pp. 85–94).
1397   https://doi.org/10.1051/limn:2008017

1398   St-Laurent, P., & Friedrichs, M. A. M. (2024a). An atlas for physical and biogeochemical
1399   conditions in the Chesapeake Bay. *SEANOE*.

1400   St-Laurent, P., & Friedrichs, M. A. M. (2024b). On the sensitivity of coastal hypoxia to its
1401   external physical forcings. *Journal of Advances in Modeling Earth Systems*, *16*(1).
1402   https://doi.org/10.1029/2023MS003845

1403   Sturdivant, S. K., Seitz, R. D., & Diaz, R. J. (2013). Effects of seasonal hypoxia on macrobenthic
1404   production and function in the Rappahannock River, Virginia, USA. *Marine Ecology*
1405   *Progress Series*, *490*, 53–68. https://doi.org/10.3354/meps10470

1406   Symonds, M. R. E., & Moussalli, A. (2011). A brief guide to model selection, multimodel
1407   inference and model averaging in behavioural ecology using Akaike's information criterion.
1408   *Behavioral Ecology and Sociobiology*, *65*(1), 13–21. https://doi.org/10.1007/s00265-010-
1409   1037-6

1410   Taylor, J. R. (2022). *An introduction to error analysis: the study of uncertainties in physical*
1411   *measurements*. MIT Press.

1412   Testa, J. M., Faganeli, J., Giani, M., Brush, M. J., De Vittor, C., Boynton, W. R., Covelli, S.,
1413   Woodland, R. J., Kovač, N., & Michael Kemp, W. (2020a). Advances in our understanding
1414   of pelagic-benthic coupling. In T. C. Malone, A. Malej, & J. Faganeli (Eds.), *Coastal*
1415   *Ecosystems in Transition: A Comparative Analysis of the Northern Adriatic and*
1416   *Chesapeake Bay* (pp. 147–175). wiley. https://doi.org/10.1002/9781119543626.ch8

1417   Testa, J. M., Faganeli, J., Giani, M., Brush, M. J., De Vittor, C., Boynton, W. R., Covelli, S.,
1418   Woodland, R. J., Kovač, N., & Michael Kemp, W. (2020b). Advances in our understanding
1419   of Pelagic-Benthic Coupling. In T. C. Malone, A. Malej, & J. Faganeli (Eds.), *Coastal*
1420   *Ecosystems in Transition: A Comparative Analysis of the Northern Adriatic and*
1421   *Chesapeake Bay* (pp. 147–175). Wiley. https://doi.org/10.1002/9781119543626.ch8

1422   Thomsen, J., Haynert, K., Wegner, K. M., & Melzner, F. (2015). Impact of seawater carbonate
1423   chemistry on the calcification of marine bivalves. *Biogeosciences*, *12*(14), 4209–4220.
1424   https://doi.org/10.5194/bg-12-4209-2015

Tumbiolo, M. L., & Downing, J. A. (1994). An empirical model for the prediction of secondary production in marine benthic invertebrate populations. *Marine Ecology Progress Series*, *114*(1), 165–174.

Tuszer-Kunc, J., Normant-Saremba, M., & Rychter, A. (2020). The combination of low salinity and low temperature can limit the colonisation success of the non-native bivalve Rangia cuneata in brackish Baltic waters. *Journal of Experimental Marine Biology and Ecology*, *524*. https://doi.org/10.1016/j.jembe.2019.151228

Vaquer-Sunyer, R., & Duarte, C. M. (2008). Thresholds of hypoxia for marine biodiversity. *Proceeds of the National Academy of Sciences*, *105*(40), 15452–15457. www.pnas.org/cgi/content/full/

Waldbusser, G. G., Hales, B., Langdon, C. J., Haley, B. A., Schrader, P., Brunner, E. L., Gray, M. W., Miller, C. A., & Gimenez, I. (2015). Saturation-state sensitivity of marine bivalve larvae to ocean acidification. *Nature Climate Change*, *5*(3), 273–280. https://doi.org/10.1038/nclimate2479

Waldbusser, G. G., Powell, E. N., & Mann, R. (2013). Ecosystem effects of shell aggregations and cycling in coastal waters: an example of Chesapeake Bay oyster reefs. *Ecology*, *94*(4), 895–903. https://doi.org/10.1890/12-1179.1

Ware, J. R., Smith, S. V, & Reaka-Kudla, M. L. (1992). Coral reefs: Sources or sinks of atmospheric CO2? *Coral Reefs*, *11*(3), 127–130.

Weisberg, S., Ranasingiie, A., Schaffner Robert J Diaz, L. C., Dauer, D. M., & Frithsen, F. B. (1997). An estuarine benthic index of biotic integrity (B-IBI) for Chesapeake Bay. *Estuaries*, *20*(1), 149–158.

Wilson, J. G., & Fleeger, J. W. (2023). Estuarine benthos. In B. C. Crump, J. M. Testa, & K. H. Dunton (Eds.), *Estuarine Ecology* (3rd ed., pp. 253–273). Wiley.

Wolf-Gladrow, D. A., Zeebe, R. E., Klaas, C., Körtzinger, A., & Dickson, A. G. (2007). Total alkalinity: The explicit conservative expression and its application to biogeochemical processes. *Marine Chemistry*, *106*(1-2 SPEC. ISS.), 287–300. https://doi.org/10.1016/j.marchem.2007.01.006

Wood, S. N. (2011). Fast stable restricted maximum likelihood and marginal likelihood estimation of semiparametric generalized linear models. *Journal of the Royal Statistical Society Series B: Statistical Methodlogy*, *73*(1), 3–36. https://academic.oup.com/jrsssb/article/73/1/3/7034726

Woodland, R. J., Buchheister, A., Latour, R. J., Lozano, C., Houde, E., Sweetman, C. J., Fabrizio, M. C., & Tuckey, T. D. (2021). Environmental drivers of forage fishes and benthic invertebrates at multiple spatial scales in a large temperate estuary. *Estuaries and Coasts*, *44*(4), 921–938. https://doi.org/10.1007/s12237-020-00835-9

Woodland, R. J., & Testa, J. M. (2020). Response of benthic biodiversity to climate-sensitive regional and local conditions in a complex estuarine system. In V. Lyubchich, Y. R. Gel, K. H. Kilbourne, T. J. Miller, N. K. Newlands, & A. B. Smith (Eds.), *Evaluating Climate Change IMpacts* (Vol. 1, pp. 87–22). CRC Press.

Zhang, Q., & Blomquist, J. D. (2018). Watershed export of fine sediment, organic carbon, and chlorophyll-a to Chesapeake Bay: Spatial and temporal patterns in 1984–2016. *Science of the Total Environment*, *619–620*, 1066–1078. https://doi.org/10.1016/j.scitotenv.2017.10.279

Zhang, Q., Fisher, T. R., Trentacoste, E. M., Buchanan, C., Gustafson, A. B., Karrh, R., Murphy, R. R., Keisman, J., Wu, C., Tian, R., Testa, J. M., & Tango, P. J. (2021). Nutrient limitation

1471   of phytoplankton in Chesapeake Bay: Development of an empirical approach for water-
1472   quality management. *Water Research*, *188*. https://doi.org/10.1016/j.watres.2020.116407
1473 Zheng, G., & DiGiacomo, P. M. (2020). Linkages between phytoplankton and bottom oxygen in
1474   the Chesapeake Bay. *Journal of Geophysical Research: Oceans*, *125*(2).
1475   https://doi.org/10.1029/2019JC015650
1476

1477